

1 Anonymous Referee #3 Received and published: 21 January 2020

2 **General Comments**

3 This study shows the complexity of haze formation processes due to coupling of  
4 transport, turbulence, stability of the lower atmosphere as well as chemical reaction.  
5 The central role of atmospheric oxidization capacity is found and their influence upon  
6 the haze generation is described. The new results of this study are well described and  
7 discussed in relation to the state-of-the-art research of haze formation. It would be  
8 helpful for the whole understanding of haze in Beijing if the influence of haze upon the  
9 radiation transfer in the atmosphere and thus the transport, turbulence and stability,  
10 which is mentioned in the introduction, or one can say the self-cleaning capacity of the  
11 atmosphere (that means feedback mechanisms) is described also. It is shown in Fig. 9  
12 only. The conclusions are a summary only and in this summary no relations to the  
13 existing knowledge / papers are given. Thus, a discussion of the results in relation of  
14 the state-of-the-art knowledge about summer haze in Beijing is required so that one can  
15 follow what is new and what is supported by this study. The conclusions in the last  
16 sentence of the abstract must be given and discussed in the chapter conclusions. The  
17 paper addresses relevant scientific questions within the scope of ACP. The paper  
18 presents novel concepts, ideas, tools and data. The scientific methods and assumptions  
19 are valid and clearly outlined so that substantial conclusions are reached. The  
20 description of experiments and calculations allow their reproduction by fellow  
21 scientists. The results are sufficient to support the interpretations and conclusions. The  
22 quality of the figures is good. The figure captions should be improved so that these are  
23 understandable without the overall manuscript: terms must be explained, description of  
24 parameters. The related work is well cited so that the authors give proper credit to  
25 related work and own new contribution. The title reflects the whole content of the paper.  
26 The abstract provides a concise and complete summary. The overall presentation is well

27 structured and clear. The language is fluent and precise but must be improved in very  
28 much details. It is necessary that a native speaker is improving the manuscript. The  
29 mathematical formulae, symbols, abbreviations, and units are generally correctly  
30 defined and used. No parts of the paper (text, formulae, figures, tables) should be  
31 reduced, combined, or eliminated. The number and quality of references is appropriate.

32 **Response:** Thank the reviewer for the constructive comments and suggestions.  
33 According to the reviewer's suggestions, we have done our best to revise our  
34 manuscript. The modifications have been highlighted in yellow or red in the following  
35 marked-up manuscript version.

36 1. The central role of atmospheric oxidization capacity is found and their influence upon  
37 the haze generation is described. The new results of this study are well described and  
38 discussed in relation to the state-of-the-art research of haze formation. It would be  
39 helpful for the whole understanding of haze in Beijing if the influence of haze upon the  
40 radiation transfer in the atmosphere and thus the transport, turbulence and stability,  
41 which is mentioned in the introduction, or one can say the self-cleaning capacity of the  
42 atmosphere (that means feedback mechanisms) is described also. It is shown in Fig. 9  
43 only.

44 **Response:** Thank the reviewer for the comments and suggestions. About this suggestion,  
45 we'd like to address that the figure 9 is an abstract graph which concluded the whole  
46 results in this paper and showed the central topic as a schematic diagram. In Fig. 9, the  
47 influence of haze upon the radiation transfer in the atmosphere and thus the transport,  
48 turbulence and stability, as well as the self-cleaning capacity of the atmosphere were  
49 schematically shown, which has been deeply discussed in section 3.2. During each stage  
50 of haze episodes, we analyzed the potential causes based on the physical and chemical  
51 processes. The physical processes involved the pollution transport and boundary layer  
52 structure effect. And the radiation transfer, stability and turbulence have been combined

53 to discuss the variation of boundary layer structure and its effects on the haze formation.  
54 For example, in the occurrence stage, we discussed the pollution causes in terms of  
55 transport, aerosol-radiation effect on stability and thus the turbulent activity in the  
56 boundary layer and further chemical processes, which was respectively shown in  
57 section 3.2.1a, 3.2.1b, and 3.2.1c. The section 3.2.3 discussed the haze diffusion stage  
58 and proposed the concept of self-cleaning capacity of the atmosphere.

59 2. The conclusions are a summary only and in this summary no relations to the existing  
60 knowledge / papers are given. Thus, a discussion of the results in relation of the state-  
61 of-the-art knowledge about summer haze in Beijing is required so that one can follow  
62 what is new and what is supported by this study.

63 Response: Thank the reviewer for the constructive suggestions. As you suggested, we  
64 have added a detailed discussion of the results in relation of the state-of-the-art  
65 knowledge about summer haze in Beijing in the chapter Conclusions. The  
66 modifications have been highlighted in yellow in the revised manuscript.

67 3. The conclusions in the last sentence of the abstract must be given and discussed in  
68 the chapter conclusions.

69 Response: Thank the reviewer for the constructive suggestions. In the last sentence of  
70 the abstract, we propose that “Even so, reducing atmospheric oxidization capacity such  
71 as strengthening the collaborative control of nitrogen oxide (NO<sub>x</sub>) and volatile organic  
72 compounds (VOCs) was urgent, as well as continuously deepening regional joint  
73 control of air pollution”. As you suggested, we have added a more detailed discussion  
74 on it in the chapter Conclusions. The modifications have been highlighted in yellow in  
75 the revised manuscript.

76 4. The figure captions should be improved so that these are understandable without the  
77 overall manuscript: terms must be explained, description of parameters.

78 Response: Thank the reviewer for the constructive suggestions.

79 Figure caption 2 has been corrected to “Figure 2. Scatter plot of the relationship  
80 between the directly measured PM<sub>2.5</sub> mass concentration (with the particulate matter  
81 analyzer of the China National Environmental Monitoring Center) and the ACSM-  
82 measured PM<sub>2.5</sub> mass concentration (the sum of the chemical constituent mass  
83 concentrations measured with the aerosol chemical speciation monitor (ACSM) and the  
84 black carbon (BC) mass concentration measured with the multiangle absorption  
85 photometer).”.

86 Figure caption 7 has been corrected to “Figure 7. Composites of the 850-hPa horizontal  
87 wind vector field (units: m s<sup>-1</sup>; white arrows), 850-hPa geopotential height field (units:  
88 m; solid lines) and 850-hPa specific humidity field (units: g kg<sup>-1</sup>; shaded colors) at 0200,  
89 0800, 1400, and 2000 (local time) on 22 and 24 July and from 26-27 July, labeled as (a)  
90 - (p). The star shows the location of the BJ site.”.

91 Figure caption 8 has been corrected to “Figure 8. The PM<sub>2.5</sub> mass concentration  
92 distribution (units: μg m<sup>-3</sup>; shaded colors) over most of China at 0200, 0800, 1400, and  
93 2000 (local time) on 22 and 24 July and from 26–27 July, labeled as (a)–(p).”.

94 Figure caption 9 has been changed to “Figure 9. Schematic diagram for the formation  
95 mechanism of haze pollution under a high atmospheric oxidization capacity in summer  
96 in Beijing (blue dashed line: atmospheric boundary layer; red solid lines: potential  
97 temperature gradient profiles; brown solid line: temporal change curve of the ozone  
98 concentration; cyan solid line: temporal change curve of the PM<sub>2.5</sub> mass concentration;  
99 gray arrow sectors: temporal change in the wind vector profiles; TKE: turbulence  
100 kinetic energy; solid dots: particulate matter in the atmosphere; droplets: water vapor).”

101 5. The language is fluent and precise but must be improved in very much details. It is  
102 necessary that a native speaker is improving the manuscript.

103 Response: Thank the reviewer for the constructive suggestions. Regarding the language,  
104 we accepted the suggestion and the revised manuscript has been improved by a native

105 speaker. The modifications have been highlighted in red in the revised manuscript.

## 106 **Specific Comments**

107 1. Figure caption 1: Set the letters a) – f) to the single instruments.

108 Response: Thank you for the suggestion. The sentence “The pictures of (a)-(f) are  
109 Microwave Radiometer, 3D Doppler Wind Lidar, CIMEL sun-photometer, Ceilometer,  
110 Aerodyne Aerosol Chemical Speciation Monitor and Multi-angle Absorption  
111 Photometer set in the BJ site.” in Figure caption 1 has been corrected to “(a: microwave  
112 radiometer; b: 3D Doppler wind lidar; c: CIMEL sun-photometer; d: ceilometer; e:  
113 Aerodyne aerosol chemical speciation monitor (ACSM); f: multiangle absorption  
114 photometer).”.

115 2. Line 581: Why diffusion stage if wind increased (line 589)? Use Dispersion stage?

116 Response: Thanks for the comments and suggestions. Regarding the statement in line  
117 589, there is some explanation we need to make. As discussed in this study, the  
118 initialization of haze in Beijing was mainly attributed to the southwest/south winds  
119 which came through the heavy polluted areas. However, the strong and air mass  
120 dissipating the air pollution in Beijing mainly came from the southeast of Beijing,  
121 shown in Figure 7(n)-(p). The southeast winds originated from the Bohai Sea and the  
122 Yellow Sea. Moreover, during this diffusion stage, the air quality of the southeast of  
123 Beijing was basically clean or much better than that in Beijing (Figure 8(n)-(p)).  
124 Therefore, strong southeast winds would not bring pollutants aggravating the pollution  
125 in Beijing instead played a role in the horizontal diffusion of the accumulated PM at the  
126 surface. On the other hand, accompanied by the horizontal diffusion, the strong solar  
127 radiation at noon reached the surface and changed the vertical temperature structure.  
128 The ABL was in extremely unstable state for both the  $\partial\theta_v/\partial z$  and  $\partial\theta_{se}/\partial z$  were negative  
129 below  $\sim 1.0$  km with values of  $-0.5$  °C/100 m and  $-2.5$  °C/100 m, respectively (Fig. 5a-  
130 b). Along with this instability, the development of turbulence in the ABL was very

131 strong and quick, with the TKE values suddenly increasing to  $\sim 3\text{-}5 \text{ m}^2 \text{ s}^{-2}$  (Fig. 5c).  
132 Accompanied by the pronounced turbulence development, the ABL continuously  
133 developed upward with the ABLH up to the  $\sim 2.5 \text{ km}$  over short time (Fig. 5d). The ABL  
134 structure quickly became extremely suitable for the vertical diffusion of pollutants, thus,  
135 the PM level sharply decreased during this time. We may haven't state it more clearly  
136 and thus we have supplemented a more detailed discussion on it. The modifications  
137 have been highlighted in yellow in the revised manuscript. Through our discussion, we  
138 think "Diffusion stage" is appropriate and also the "Dispersion stage".

139 3. Technical corrections Line 727, 873: doi number is missing. Lines 770, 772: the  
140 reference is incomplete. Lines 856, 858, 859: improve the format.

141 Response: Thanks for the reviewer's suggestions.

142 The reference in Line 727 has been corrected to "Ainsworth, E. A., Yendrek, C. R.,  
143 Sitch, S., Collins, W. J., and Emberson, L. D.: The Effects of Tropospheric Ozone on  
144 Net Primary Productivity and Implications for Climate Change, Annual Review of Plant  
145 Biology, 63, 637-661, <https://doi.org/10.1146/annurev-arplant-042110-103829>, 2012.".

146 The reference in Line 873 has been corrected to "Su, F., Gao, Q., Zhang, Z., Ren, Z.,  
147 and Yang, X.: Transport Pathways of Pollutants from Outside in Atmosphere Boundary  
148 Layer, Res. Environ. Sci., 17(1), 26-29,40, [https://doi.org/10.3321/j.issn:1001-](https://doi.org/10.3321/j.issn:1001-6929.2004.01.005)  
149 [6929.2004.01.005](https://doi.org/10.3321/j.issn:1001-6929.2004.01.005), 2004.".

150 Through our discussion, we have decided to delete the reference in Line 770.

151 The reference in Line 772 has been corrected to "Gregory, L.: Cimel Sunphotometer  
152 (CSPHOT) Handbook, Office of Scientific & Technical Information Technical Reports,  
153 <https://doi.org/10.2172/1020262>, 2011.".

154 The reference in Lines 856-857 has been corrected to "Richards, L. W.: comments on  
155 the oxidation of NO<sub>2</sub> to nitrate- day and night, Atmos. Environ., 17, 397-402,  
156 [https://doi.org/10.1016/0004-6981\(83\)90057-4](https://doi.org/10.1016/0004-6981(83)90057-4), 1983.".

157 The reference in Lines 858-859 has been corrected to “Russell, A. G., Cass, G. R., and  
158 Seinfeld, J. H.: On some aspects of nighttime atmospheric chemistry, Environ. Sci.  
159 Technol., 20, 1167-1172, <https://doi.org/10.1021/es00153a013>, 1986.”.

160

161 Anonymous Referee #1 Received and published: 14 February 2020

## 162 **General Comments**

163 This paper focusses in detail on the physical and chemical processes involved in 2  
164 extreme summer haze events in Beijing. In particular, the paper looks into the coupling  
165 between the build of ozone and the resultant feedbacks on PM concentrations through  
166 the impacts on the oxidative capacity of the atmosphere. Overall, the paper also  
167 concludes the strong role that regional transport plays in such events. Finally, the paper  
168 also concludes that meteorology plays an important role in the self-cleaning effect of  
169 the atmosphere that ends such pollution events. Overall this paper is well written and  
170 uses robust methodology to support the above conclusions. However there are some  
171 relatively minor corrections that need addressing before publication can be  
172 recommended. In particular, there were a number of points in the paper where sentences  
173 where repeated. A number of these have been pointed out below but please ensure all  
174 are corrected in the revised manuscript.

175 **Response:** Thank the reviewer for the positive comments and constructive suggestions.  
176 As the reviewer pointed out that there are some relatively minor corrections listed below,  
177 we have done our best to answer the minor comments and revise our manuscript. The  
178 specific answers have been listed below. The modifications have been highlighted in  
179 blue in the following marked-up manuscript.

## 180 **Minor Comments**

181 1. Page 1, Line 18: Please remove the ~ symbol at the end of the line. No need to put  
182 approximations when quoting a range.

183 Response: Thank the reviewer for the constructive suggestions. We have corrected it as  
184 well as other similar problems in the revised manuscript.

185 2. Page 10, line 232: No need to reference GB3095-2012 again as you have already  
186 done this above.

187 Response: Thank the reviewer for the constructive suggestions. We have corrected it in  
188 the revised manuscript. This sentence was corrected to “Besides, an ozone pollution  
189 day is any day when the hourly mean O<sub>3</sub> concentration is higher than 160 μg m<sup>-3</sup>; thus,  
190 during the observation periods, each day was a severe ozone pollution day.”.

191 3. Page 15, Line 294: Please correct origin to originate.

192 Response: Thank the reviewer for the constructive suggestions. We have corrected it in  
193 the revised manuscript.

194 4. Page 15, Line 295: Please correct wee hours to early hours.

195 Response: Thank the reviewer for the constructive suggestions. We have corrected it in  
196 the revised manuscript.

197 5. Page 15, Line 303: There is a lot of repetition in this sentence. Please simplify to  
198 ‘Under persistent southerly winds, water vapor was carried to Beijing forming a  
199 moisture transport channel which strengthened.’

200 Response: Thank the reviewer for the constructive suggestions. We have corrected it in  
201 the revised manuscript. According to the suggestion, this sentence has been corrected  
202 to “Under persistent southerly winds, water vapor was carried to Beijing forming a  
203 moisture transport channel which increasingly intensified.”.

204 6. Page 15, Line 305: Please remove conspicuous and just say increase.

205 Response: Thank the reviewer for the constructive suggestions. We have corrected it in  
206 the revised manuscript.

207 7. Page 22, Line 481: I don’t understand why the phrasing ‘The same work . . .’ Is used  
208 here. Please define.



209 Response: Thank the reviewer for the constructive suggestions. We may haven't state  
210 it clearly and thus we have corrected it in the revised manuscript. This sentence was  
211 corrected to "Similarly, ambient water vapor was also not conductive to dispersed,  
212 which explained the extremely high humidity during this period."

213

214

215

216

217

218

219

220

221

222

223

224

225

226

227

228

229

230

231

232

233

234

235 **Haze pollution under a high atmospheric oxidization capacity in summer in**  
236 **Beijing: Insights into formation mechanism of atmospheric physicochemical**  
237 **processes**

238 Dandan Zhao<sup>†1,2</sup>; Guangjing Liu<sup>†3,1</sup>; Jinyuan Xin<sup>\*1,2,4</sup>; Jiannong Quan<sup>5</sup>; Yuesi Wang<sup>1</sup>; Xin Wang<sup>3</sup>;  
239 Lindong Dai<sup>1</sup>; Wenkang Gao<sup>1</sup>; Guiqian Tang<sup>1</sup>; Bo Hu<sup>1</sup>; Yongxiang Ma<sup>1</sup>; Xiaoyan Wu<sup>1</sup>; Lili  
240 Wang<sup>1</sup>; Zirui Liu<sup>1</sup>; Fangkun Wu<sup>1</sup>

241 1 State Key Laboratory of Atmospheric Boundary Layer Physics and Atmospheric Chemistry (LAPC),  
242 Institute of Atmospheric Physics, Chinese Academy of Sciences, Beijing 100029, China

243 2 University of Chinese Academy of Sciences, Beijing 100049, China

244 3 College of Atmospheric Sciences, Lanzhou University, Lanzhou 730000, China.

245 4 Collaborative Innovation Center on Forecast and Evaluation of Meteorological Disasters, Nanjing  
246 University of Information Science and Technology, Nanjing 210044

247 5 Institute of Urban Meteorology, Chinese Meteorological Administration, Beijing, China

248 (†) These authors contributed equally to this study.

249 (\*) Correspondence: Jinyuan Xin ([xjy@mail.iap.ac.cn](mailto:xjy@mail.iap.ac.cn))

250 **Abstract:** Under a high atmospheric oxidization capacity, the synergistic effect of the  
251 physicochemical processes in the atmospheric boundary layer (ABL) caused summer  
252 haze pollution in Beijing. The south/southwest areas, generally 60-300 km away from  
253 Beijing, were seriously polluted, in contrast to Beijing, which remained clean.  
254 Southerly winds moving faster than 20-30 km h<sup>-1</sup> since the early morning primarily  
255 caused haze pollution initiation. The PM<sub>2.5</sub> (particulate matter with a dynamic  
256 equivalent diameter smaller than 2.5 μm) level increased to 75 μg m<sup>-3</sup> over several hours  
257 during the daytime, which was simultaneously affected by the ABL structure.  
258 Additionally, the O<sub>3</sub> concentration was quite high during the daytime (250 μg m<sup>-3</sup>),  
259 corresponding to a high atmospheric oxidation capacity. Much sulfate and nitrate were  
260 produced through active atmospheric chemical processes, with sulfur oxidation ratios  
261 (SORs) up to ~0.76 and nitrogen oxidation ratios (NORs) increasing from 0.09 to 0.26,  
262 which further facilitated particulate matter (PM) level enhancement. However, the  
263 increase in sulfate was mainly linked to southerly transport. At midnight, the PM<sub>2.5</sub>

264 concentration sharply increased from 75 to 150  $\mu\text{g m}^{-3}$  over 4 hours and remained at its  
265 highest level until the next morning. Under an extremely stable ABL structure,  
266 secondary aerosol formation dominated by nitrate was quite intense, driving the haze  
267 pollution outbreak. The PM levels in the south/southeast area of Beijing were  
268 significantly lower than those in Beijing at this time, even below air quality standards;  
269 thus, the contribution of pollution transport had almost disappeared. With the formation  
270 of a nocturnal stable boundary layer (NSBL) at an altitude ranging from 0-0.3 km, the  
271 extremely low turbulence kinetic energy (TKE) ranging from 0-0.05  $\text{m}^2 \text{s}^{-2}$  inhibited  
272 the spread of particles and moisture, ultimately resulting in elevated near-surface  $\text{PM}_{2.5}$   
273 and relative humidity (~90%) levels. Due to the very high humidity and ambient  
274 oxidization capacity, NOR rapidly increased from 0.26 to 0.60, and heterogeneous  
275 hydrolysis reactions at the moist particle surface were very notable. The nitrate  
276 concentration steeply increased from 11.6 to 57.8  $\mu\text{g m}^{-3}$ , while the sulfate and organics  
277 concentrations slightly increased by 6.1 and 3.1  $\mu\text{g m}^{-3}$ , respectively. With clean and  
278 strong winds passing through Beijing, the stable ABL dissipated with the potential  
279 temperature gradient becoming negative and the ABL height (ABLH) increasing to ~2.5  
280 km. The high turbulence activity with a TKE ranging from 3-5  $\text{m}^2 \text{s}^{-2}$  notably promoted  
281 pollution diffusion. The self-cleaning capacity of the atmosphere is commonly  
282 responsible for air pollution dispersion. However, reducing the atmospheric oxidization  
283 capacity, through strengthening collaborative control of nitrogen oxide (NO<sub>x</sub>) and  
284 volatile organic compounds (VOCs), is urgent, as well as continuously deepening  
285 regional joint air pollution control.

## 286 1 Introduction

287 Due to a series of stringent emission control measures (China's State Council 2013  
288 Action Plan for Air Pollution Prevention and Control available at  
289 <http://gov.cn/zwggk/2013-09/12/>), including shutting down heavily polluting factories and  
290 replacing coal with clean energy sources, the annual mean  $\text{PM}_{2.5}$  (particulate matter  
291 with a dynamic equivalent diameter smaller than 2.5  $\mu\text{m}$ ) concentration in major  
292 regions, especially in Beijing, has continuously decreased in recent years (Chen et al.,

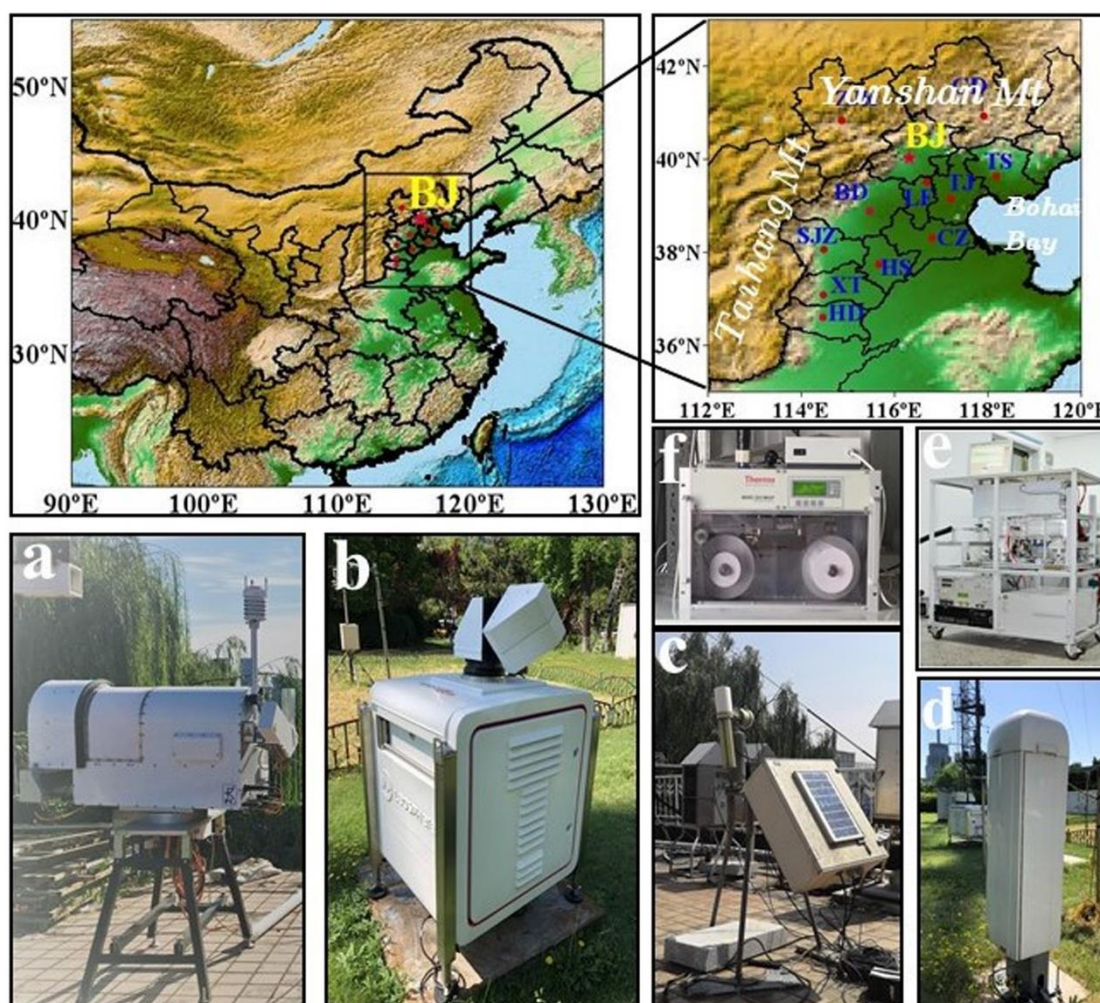
293 2019; Liu et al., 2019a; Cheng et al., 2019a; Ding et al., 2019). However, the ground-  
294 level O<sub>3</sub> concentration across China has increased rapidly in recent years, especially in  
295 summer, despite recent reductions in SO<sub>2</sub> and nitrogen oxide (NO<sub>x</sub>) emissions (Chen  
296 et al., 2018; Anger et al., 2016; Wang et al., 2018; Wang et al., 2017b). This discrepancy  
297 in the variation trend between O<sub>3</sub> and PM<sub>2.5</sub> may be attributed to inappropriate reduction  
298 ratios of NO<sub>x</sub> and volatile organic compounds (VOCs) in PM<sub>2.5</sub>-control-oriented  
299 emission reduction measures, which mainly focus on NO<sub>x</sub> reduction (Liu et al., 2013a;  
300 Cheng et al., 2019b). In addition, a number of studies have demonstrated that reducing  
301 ambient particles influences surface ozone generation by affecting heterogeneous  
302 reactions and decreasing the photodecomposition rate (O<sub>3</sub> and its precursors) through  
303 aerosol-radiation interactions (Liu et al., 2019b; Wang et al., 2019b; He and Carmichael,  
304 1999; Dickerson et al., 1997; Tie et al., 2001; Martin et al., 2003; Tie et al., 2005).  
305 Recently, even though the PM<sub>2.5</sub> level in Beijing has generally been low due to stringent  
306 emission control measures, several haze pollution episodes with  
307 alternating/synchronous high ozone concentrations have still occurred in the summer  
308 of 2019. Regarding the causes of particulate matter (PM) pollution, numerous previous  
309 studies have reported that stationary synoptic conditions, local emissions and regional  
310 transport, an adverse atmospheric boundary layer (ABL) structure and meteorological  
311 conditions as well as secondary aerosol formation are major factors in haze pollution  
312 formation (Li et al., 2019; Sun et al., 2012; Wang et al., 2016; Liu et al., 2019c; Huang  
313 et al., 2017; Luan et al., 2018; Han et al., 2019). Huang et al. (2017) demonstrated that  
314 haze pollution in Beijing-Tianjin-Hebei usually occurred when air masses originating  
315 from polluted industrial regions in the south prevailed and are characterized by high  
316 PM<sub>2.5</sub> loadings with considerable contributions from secondary aerosols. Bi et al. (2017)  
317 stated that the strong winds and vertical mixing in the daytime scavenged pollution, and  
318 the weak winds and stable inversion layer in the nighttime promoted air pollutant  
319 accumulation near the surface. Zhong et al. (2018) showed that positive ABL  
320 meteorological feedback on the PM<sub>2.5</sub> mass concentration explains over 70% of the  
321 outbreak of pollution. Zhao et al. (2019) also revealed that the constant feedback effect

322 between aerosol radiative forcing and ABL stability continually reduced the  
323 atmospheric environmental capacity and aggravated air pollution. The dominant PM  
324 components, including sulfate, nitrate, ammonium, and organics (Org), are mostly  
325 formed via the homogeneous/heterogeneous reactions of gas-phase precursors in the  
326 atmosphere (Orrling et al., 2011; Wang et al., 2016) and account for over 50% of the  
327 PM<sub>2.5</sub> mass (Wang et al., 2013; Liu et al., 2019a; Sun et al., 2015; Yao et al., 2002).  
328 Ming et al. (2017) proved that the contribution of secondary aerosol formation during  
329 haze pollution episodes was much higher than that before and after haze pollution  
330 episodes.

331 Although the causes of high PM<sub>2.5</sub> loadings have been widely examined, most of  
332 these studies have focused on haze pollution in winter and only involved one or several  
333 key factors. In summer in Beijing, with high solar radiation, O<sub>3</sub> can be quickly formed  
334 via photochemical reactions among precursors, including volatile organic compounds  
335 (VOCs) and nitrogen oxides (NO<sub>x</sub>), which contributes to an increase in the ambient  
336 oxidizing capacity (Wang et al., 2017c; Ainsworth et al., 2012; Hassan et al., 2013;  
337 Trainer et al., 2000; Sillman, 1999). Meteorological conditions, including solar  
338 radiation, temperature, relative humidity, wind speed and direction, and cloud cover,  
339 also play an important role in short-term ozone variations, further affecting the  
340 atmospheric oxidization capacity (Lu et al., 2019; Cheng et al., 2019b; Toh et al., 2013;  
341 Wang et al., 2017d; Zeng et al., 2018). As ozone pollution is increasingly becoming  
342 prominent and the atmospheric oxidation capacity is gradually increasing, the  
343 formation mechanism of haze pollution under a high atmospheric oxidization capacity  
344 needs to be concerned. Previous studies have demonstrated that intense atmospheric  
345 photochemical reactions in summer enhanced secondary aerosol formation and led to  
346 the synchronous occurrence of high PM<sub>2.5</sub> and O<sub>3</sub> concentrations on a regional scale  
347 (Pathak et al., 2009; Wang et al., 2016; Shi et al., 2015). Nevertheless, the mechanisms  
348 of how the overall regional transport, ABL structure, meteorological conditions and  
349 secondary aerosol formation interact to quantitatively influence haze pollution under  
350 a high atmospheric oxidization capacity in summer remain unclear. Therefore, by

351 **closely monitoring** air temperature and relative **and** absolute humidity profiles, vertical  
 352 velocity and horizontal wind vector profiles, atmospheric backscattering coefficient  
 353 (BSC) profiles and **the ABL height (ABLH)**, as well as **the** mass concentration and  
 354 composition of PM<sub>2.5</sub>, aerosol optical depth (AOD) and mass concentrations of gas  
 355 pollutants including O<sub>3</sub>, SO<sub>2</sub>, and NO<sub>2</sub>, this paper comprehensively **examines** the  
 356 formation mechanism of haze pollution under **a high** ambient oxidization capacity  
 357 insights into atmospheric physics and chemistry **to propose select** recommendations  
 358 for model **forecasting** and cause analysis of complex air pollution **in summer in Beijing**.

359 **2 Instruments and data**



360  
 361 Figure 1. The geographical location of Beijing city (BJ) marked **with** a red star as well as  
 362 surrounding regions and **relevant** measurement instruments **implemented** in this paper. **The left-**  
 363 **top** panel is the topographic distribution of most of China with Beijing and surrounding areas  
 364 **marked**, and **the** right-top panel is the topographic distribution of the Beijing-Tianjin-Hebei

365 (BTH) region, with the Yanshan Mountains to the north, the Taihang Mountains to the west,  
366 and Bohai Bay to the east. The blue words are abbreviations of city names in the BTH region  
367 (a: microwave radiometer; b: 3D Doppler wind lidar; c: CIMEL sun-photometer; d: ceilometer;  
368 e: Aerodyne aerosol chemical speciation monitor (ACSM); f: multiangle absorption  
369 photometer).

## 370 2.1 Instruments and related data

371 The observation site was located at the Tower Branch of the Institute of  
372 Atmospheric Physics (IAP), Chinese Academy of Sciences (39°58'N, 116°22'E;  
373 altitude: 58 m). The IAP site is located at the intersection of the north ring-3 and north  
374 ring-4 roads in Beijing, China, among educational, commercial and residential areas,  
375 and represents a typical urban site in Beijing (hereinafter BJ site). All the sampling  
376 instruments are placed at the same location to conduct simultaneous monitoring. All the  
377 data used in this paper were recorded from July 22 to 27, 2019, and are reported in  
378 Beijing Standard Time.

379 Air temperature and relative and absolute humidity profiles were collected with a  
380 microwave radiometer (RPG-HATPRO-G5 0030109, Germany). The microwave  
381 radiometer (hereinafter MWR) produces profiles with a resolution ranging from 10-30  
382 m up to 0.5 km, profiles with a resolution ranging from 40-70 m between 0.5 and 2.5  
383 km and profiles with a resolution ranging from 100-200 m from 2 to 10 km at a temporal  
384 resolution of 1 s. A detailed description of RPG-HATPRO-type instruments can be  
385 found at <http://www.radiometer-physics.de>.

386 Vertical wind speed and horizontal wind vector profiles were retrieved with a 3D  
387 Doppler wind lidar (Windcube 100s, Leosphere, France). The wind measurement  
388 results have a spatial resolution ranging from 1-20 m up to 0.3 km and one of 25 m  
389 from 0.3 to 3 km, with a temporal resolution of 1 s. More instrument details can be  
390 found on [www.leosphere.com](http://www.leosphere.com).

391 A ceilometer (CL51, Vaisala, Finland) recorded atmospheric BSC profiles. The  
392 CL51 ceilometer digitally sampled the return backscattering signal from 0 to 100  $\mu$ s  
393 and provided BSC profiles with a spatial resolution of 10 m from the ground to a height

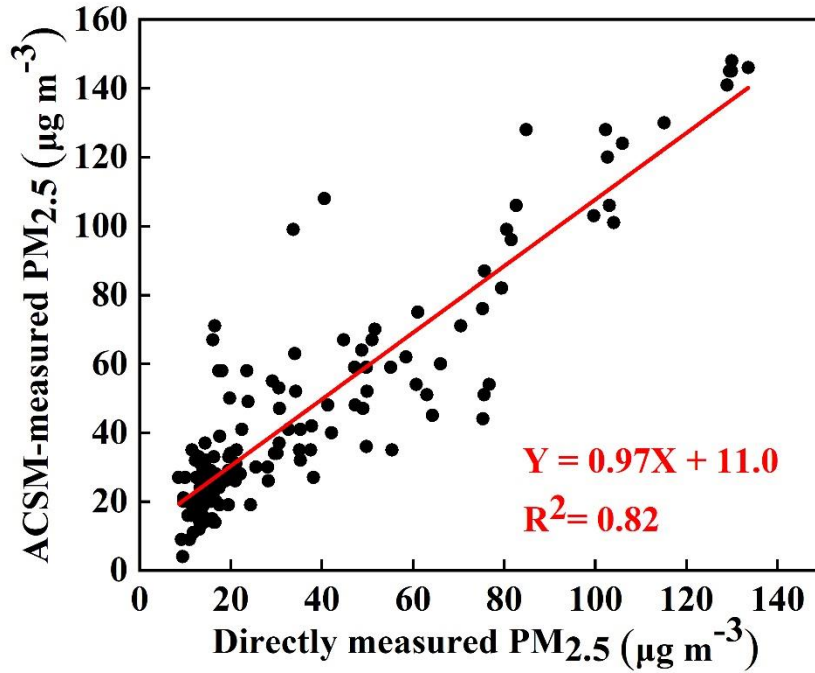
394 of 15 km. As PM mostly suspends in the ABL and is barely present in the free  
395 atmosphere, the ABLH was determined by the sharp change in the negative gradient of  
396 BSC profiles (Muenkel et al., 2007). More detailed information on ABLH calculation  
397 and screening can be found in previous studies (Tang et al., 2016; Zhu et al., 2018).

398 The aerosol optical depth (AOD) is observed by a CIMEL sun-photometer (CE318,  
399 France), and the AOD at 500 nm is adopted in this paper. The CE318 instrument is a  
400 multichannel, automatic sun-and-sky-scanning radiometer and only acquires  
401 measurements during daylight hours (with the sun above the horizon). Detailed  
402 information on the AOD inversion method and the CE318 instrument have been  
403 presented in Gregory (2011).

404 The real-time hourly mean PM<sub>2.5</sub>, PM<sub>10</sub>, O<sub>3</sub>, NO<sub>2</sub> and SO<sub>2</sub> ground levels were  
405 downloaded from the China National Environmental Monitoring Center (CNEMC)  
406 (available at <http://106.37.208.233:20035/>). All operational procedures are strictly  
407 conducted following the Specification of Environmental Air Quality Automatic  
408 Monitoring Technology (HJ/T193-2005, available at  
409 [http://kjs.mep.gov.cn/hjbhbz/bzwb/dqhbh/jcgfffbz/200601/t20060101\\_71675.htm](http://kjs.mep.gov.cn/hjbhbz/bzwb/dqhbh/jcgfffbz/200601/t20060101_71675.htm)).

410 The PM chemical species, including the organics (Org), sulfate (SO<sub>4</sub><sup>2-</sup>), nitrate (NO<sub>3</sub><sup>-</sup>),  
411 ammonium (NH<sub>4</sub><sup>+</sup>) and chloride (Cl<sup>-</sup>), were measured every hour with an aerosol  
412 chemical speciation monitor (ACSM). More detailed descriptions of the ACSM have  
413 been given in Ng et al. (2011). The black carbon (BC) mass concentration was measured  
414 with a multiangle absorption photometer (MAAP5012, Thermo Electron). A more  
415 detailed description of the MAAP5012 instrument can be found in Petzold and  
416 Schonlinner (2004). As shown in Fig. 2, the ACSM-measured PM<sub>2.5</sub> mass concentration  
417 (=organics + sulfate + nitrate + ammonium + chloride + BC) tracked the online PM<sub>2.5</sub>  
418 mass concentration well, which was directly measured with a PM analyzer (from  
419 CNEMC), with a correlation coefficient (R<sup>2</sup>) of 0.82. On average, the ACSM-measured  
420 PM<sub>2.5</sub> mass concentration accounts for 80% of the online PM<sub>2.5</sub> mass concentration. All  
421 chemical compositions measured by the ACSM, including organics, sulfate, nitrate  
422 ammonium and chloride, as well as BC, represent the dominant species of PM<sub>2.5</sub>.





423

424 Figure 2. Scatter plot of the relationship between the directly measured PM<sub>2.5</sub> mass  
 425 concentration (with the particulate matter analyzer of the China National Environmental  
 426 Monitoring Center) and the ACSM-measured PM<sub>2.5</sub> mass concentration (the sum of the  
 427 chemical constituent mass concentrations measured with the aerosol chemical speciation  
 428 monitor (ACSM) and the black carbon (BC) mass concentration measured with the multiangle  
 429 absorption photometer).

## 430 2.2 Other datasets

431 The virtual potential temperature ( $\theta_v$ ) and pseudoequivalent potential temperature  
 432 ( $\theta_{se}$ ) are calculated by Eqs. (1) and (2), respectively:

$$433 \theta_v = T(1 + 0.608q)\left(\frac{1000}{p}\right)^{0.286} \quad (1)$$

$$434 \theta_{se} = T\left(\frac{1000}{p}\right)^{0.286} \exp\left(\frac{r_s L_v}{C_{pd} T}\right) \quad (2)$$

435 where  $T$  is the air temperature,  $q$  is the specific humidity,  $p$  is the air pressure,  $r_s$  is the  
 436 saturation mixing ratio,  $L_v$  is the latent heat of vaporization, i.e.,  $2.5 \times 10^6 \text{ J kg}^{-1}$ , and  $C_{pd}$   
 437 is the specific heat of air, i.e.,  $1005 \text{ J kg}^{-1} \text{ K}^{-1}$ . All the relevant parameters can be  
 438 calculated from the MWR-measured temperature and humidity profile data, and the  $\theta_v$   
 439 and  $\theta_{se}$  values at the different altitudes can then be further obtained. The hourly  
 440 turbulence kinetic energy (TKE) is calculated as:

441  $TKE = 0.5 \times (\delta_u^2 + \delta_v^2 + \delta_w^2)$  (3)

442 The one-hour vertical velocity standard deviation ( $\delta_w^2$ ) and the one-hour horizontal  
 443 wind standard deviation ( $\delta_u^2$  and  $\delta_v^2$ ) are calculated with Eqs. (4), (5) and (6),  
 444 respectively:

445  $\delta_w^2 = \frac{1}{N-1} \sum_{i=1}^N (w_i - \bar{w})^2$  (4)

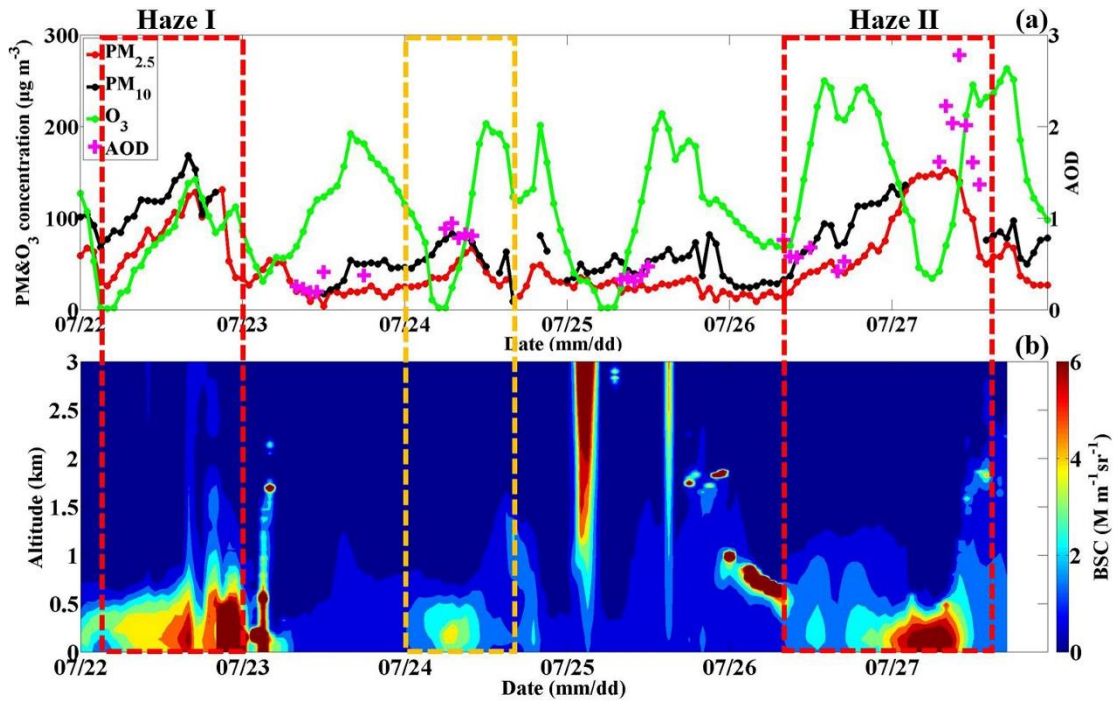
446  $\delta_u^2 = \frac{1}{N-1} \sum_{i=1}^N (u_i - \bar{u})^2$  (5)

447  $\delta_v^2 = \frac{1}{N-1} \sum_{i=1}^N (v_i - \bar{v})^2$  (6)

448 where N is the number of records each hour,  $w_i$  is the  $i$ th vertical wind velocity ( $m s^{-1}$ ),  
 449  $u_i(v_i)$  is the  $i$ th horizontal wind speed ( $m s^{-1}$ ),  $\bar{w}$  is the mean vertical wind speed ( $m$   
 450  $s^{-1}$ ), and  $\bar{u}(\bar{v})$  is the mean horizontal wind speed ( $m s^{-1}$ ) (Wang et al., 2019a; Banta  
 451 et al., 2006). Atmospheric reanalysis data from the National Centers for Environmental  
 452 Prediction (NCEP) were collected 4 times a day at 0200, 0800, 1400, and 2000 (local  
 453 time) at a horizontal resolution of  $2.5^\circ \times 2.5^\circ$ .

454 **3 Results and discussion**

455 **3.1 Typical air pollution episodes in summer in Beijing**



456  
 457 Figure 3. (a) Temporal variations in the PM<sub>2.5</sub>, PM<sub>10</sub> and O<sub>3</sub> mass concentrations as well as in  
 458 the aerosol optical depth (AOD) at the BJ site from July 22-27, 2019; (b) temporal variations

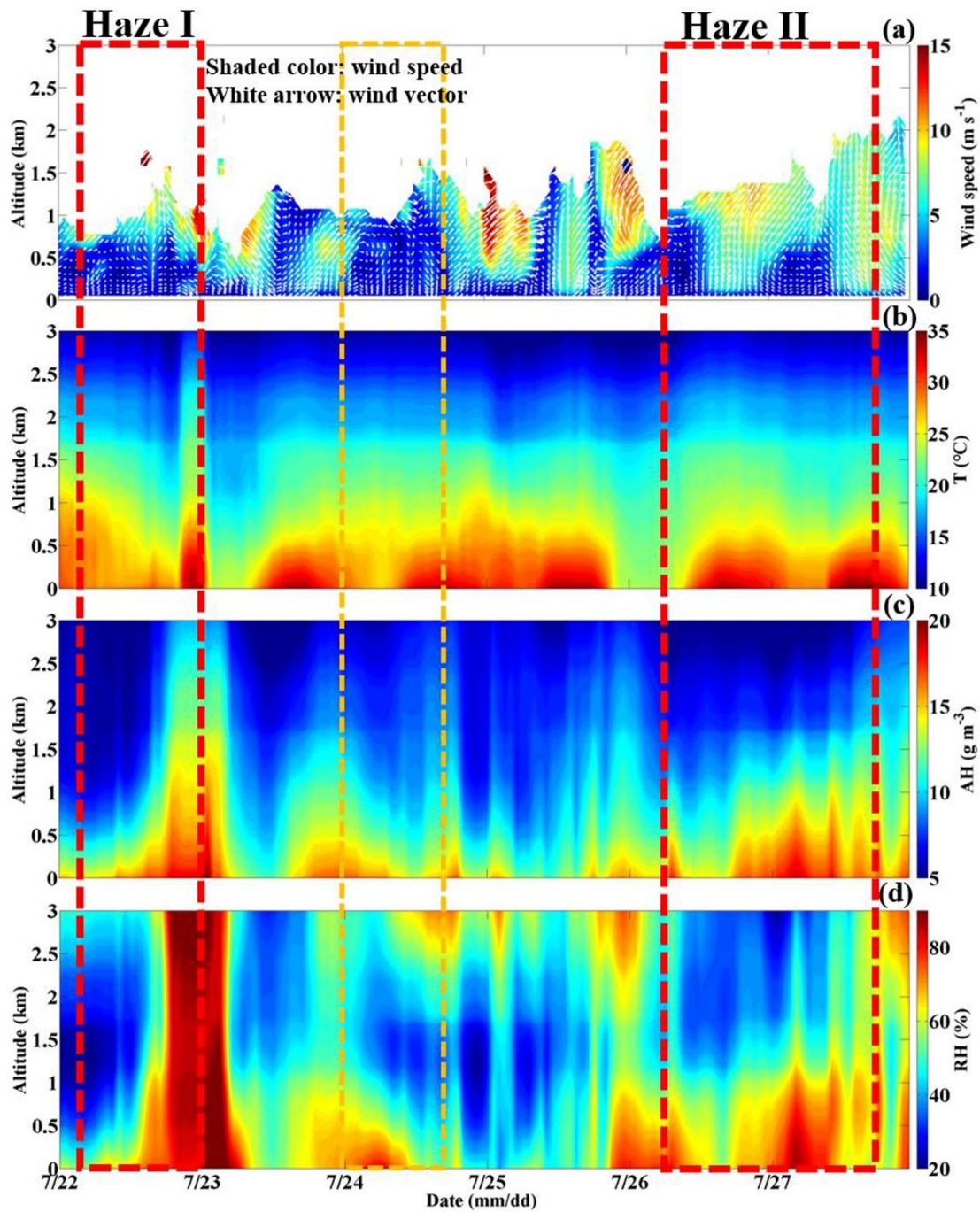
459 in the vertical atmospheric backscattering coefficient (BSC) profiles at the BJ site from July  
460 22-27, 2019 (the yellow mark represents the light-haze pollution period, and the red mark  
461 represents the heavy-haze pollution episode).

462 Considering that the daily mean PM<sub>2.5</sub> mass concentration on both 22 July and  
463 from 26-27 July exceeded the national secondary standard (75 µg m<sup>-3</sup>) (GB3095-2012)  
464 with maximum hourly averages up to 131 and 152 µg m<sup>-3</sup>, respectively, two severe PM  
465 pollution processes occurred, defined as Haze I and Haze II. During these two haze  
466 periods, high atmospheric BSC levels mainly occurred below an altitude of 0.5 km,  
467 with values ranging from 4-6 M m<sup>-1</sup> sr<sup>-1</sup>. This reflects the vertical distribution of  
468 ambient particles from the aspect of aerosol scattering to a certain degree, namely, only  
469 do the suspended particles concentrated in the lower layer of the atmosphere. Besides,  
470 an ozone pollution day is any day when the hourly mean O<sub>3</sub> concentration is higher than  
471 160 µg m<sup>-3</sup>; thus, during the observation periods, each day was a severe ozone pollution  
472 day. As reported by the Ministry of Ecology and Environment, in 2018, the number of  
473 motor vehicles reached 327 million, up by 5.5% year-on-year (available at  
474 [http://www.mee.gov.cn/xxgk2018/xxgk/xxgk15/201909/t20190904\\_732374.html](http://www.mee.gov.cn/xxgk2018/xxgk/xxgk15/201909/t20190904_732374.html)).

475 Although stringent pollution control measures have been implemented regarding  
476 factories, motor vehicles still discharge large amounts of primary pollutants into the  
477 atmosphere, including NO<sub>x</sub>, HC, VOCs, and CO. Under high solar radiation and  
478 temperature levels in summer, photochemical processes are prominent, contributing to  
479 a high O<sub>3</sub> concentration along with many highly reactive radicals, which further  
480 enhance the oxidizing capacity of the atmosphere (Frischer et al., 1999; Sharma et al.,  
481 2013). Haze pollution under a high atmospheric oxidation capacity had likely occurred  
482 on 22 July and from 26-27 July. Generally, due to the stringent pollutant emission  
483 control measures, the emission of primary aerosols is low, with a very low PM<sub>2.5</sub> level  
484 in summer in Beijing. The sudden elevated ambient particle concentration (the Haze I  
485 and Haze II periods) resulted in the worst PM pollution in Beijing that summer and has  
486 been widely concerned by the public. Thus, the formation mechanism of the Haze I and  
487 Haze II periods during which the PM<sub>2.5</sub> and O<sub>3</sub> concentrations were

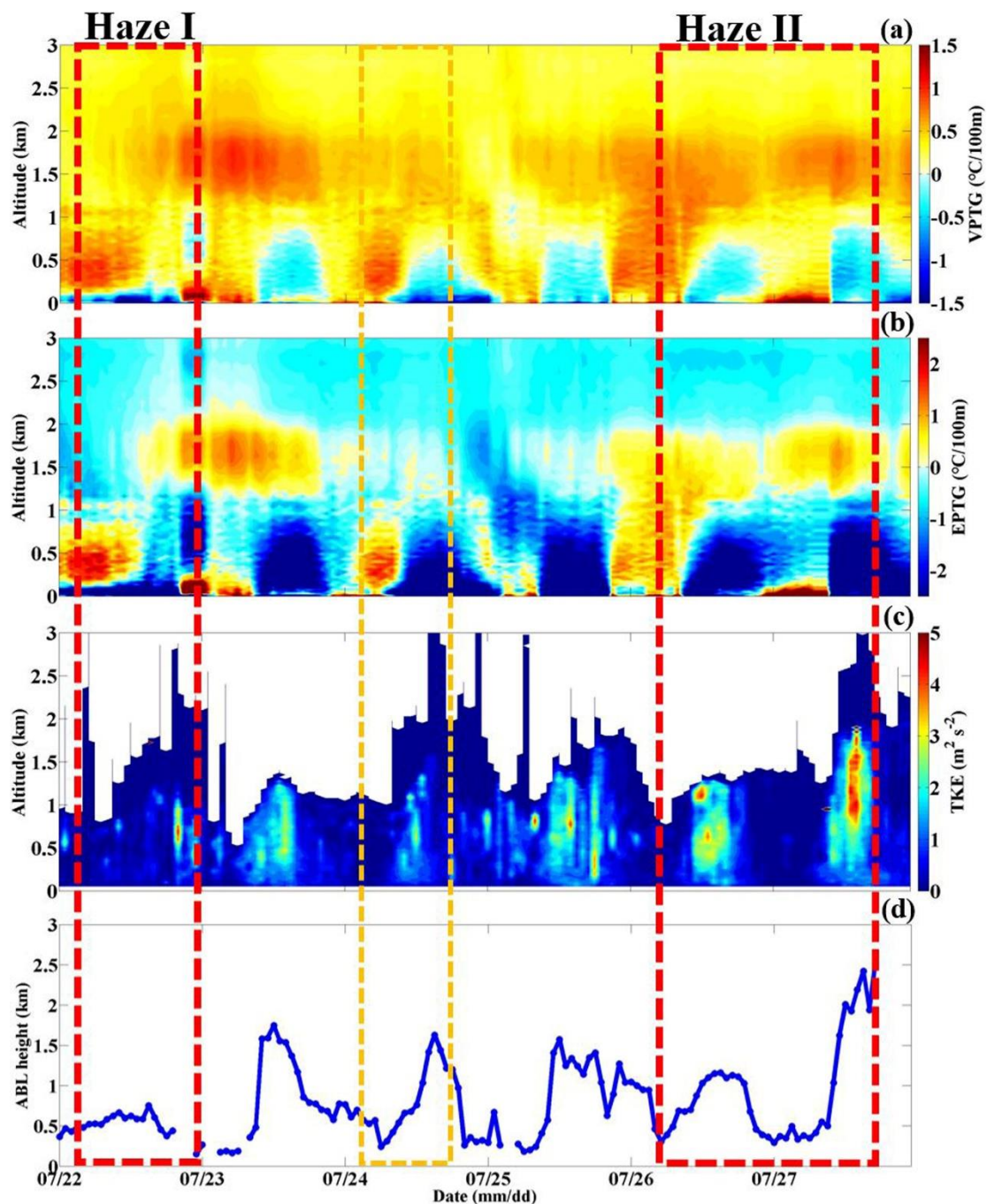
488 simultaneously/alternately high should be **systematically examined**. The key point is to  
489 determine the oxidation capacity of **the** regional atmosphere and to clarify the formation  
490 mechanism of secondary aerosols. **In addition**, the occurrence and evolution patterns of  
491 **these** two haze processes were different, which could refer to the diverse accumulation  
492 mechanisms, regional transfer contributions, ABL structures, and removal processes.  
493 **Therefore**, by clarifying the various pollution processes, it **should be** possible to  
494 **determine** the leading factors of **these** haze **phenomena** in Beijing in summer. In  
495 **summary**, we **will examine** the haze pollution **causes** under **a high** atmospheric  
496 oxidization capacity in terms of the **physical processes**, such as **pollutant** sources and  
497 sinks and ABL structure influence, and **chemical processes**, **namely**, aerosol  
498 transformation **processes**.

### 499 **3.2 The formation mechanism of haze pollution in summer in Beijing**



500

501 Figure 4. Temporal variation in the vertical profiles of the (a) horizontal wind vector (the white  
 502 arrows denote wind vectors), (b) temperature (T), (c) absolute humidity (AH), and (d) relative  
 503 humidity (RH) at the BJ site from July 22-27, 2019 (the yellow mark represents the light-haze  
 504 pollution period, and the red mark represents the heavy-haze pollution episode).

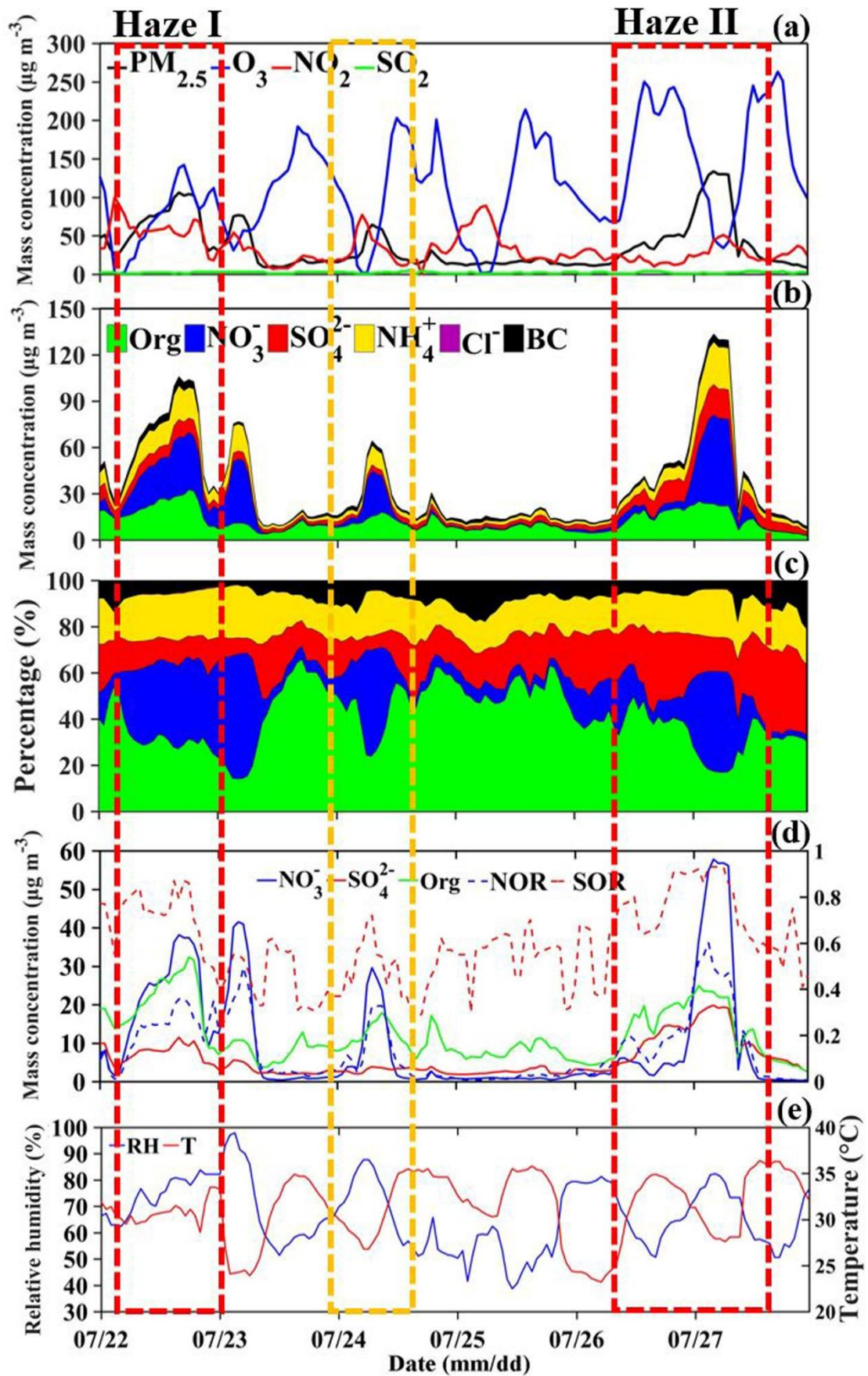


505

506 Figure 5. Temporal variation in the vertical profiles of the (a) virtual potential temperature  
 507 gradient (VPTG:  $\partial\theta_v/\partial z$ ), (b) pseudoequivalent potential temperature gradient (EPTG:  $\partial\theta_{se}/\partial z$ )  
 508 and (c) turbulent kinetic energy (TKE), along with the corresponding (d) atmospheric boundary  
 509 layer height (ABLH) at the BJ site from July 22-27, 2019 (the yellow mark represents the light-  
 510 haze pollution period, and the red mark represents the heavy-haze pollution episode).

511

512



513

514 Figure 6. Temporal variation in the (a)  $PM_{2.5}$ ,  $O_3$ ,  $NO_2$  and  $SO_2$  mass concentrations, (b)  $PM_{2.5}$

515 chemical **composition**, including **organics** (Org), sulfate ( $\text{SO}_4^{2-}$ ), nitrate ( $\text{NO}_3^-$ ), ammonium salt  
516 ( $\text{NH}_4^+$ ), chlorine salt ( $\text{Cl}^-$ ) and black carbon (BC) **at** the BJ site **from** July 22-27, 2019. (c)  
517 Temporal variation **in** the relative contributions of **the** chemical **components** to **the**  $\text{PM}_{2.5}$  mass  
518 concentration **at** the BJ site **from** July 22-27, 2019. (d) Temporal variation **in** **the** mass  
519 concentrations of **the** dominant  $\text{PM}_{2.5}$  chemical **components**, sulfur oxidation ratio (SOR) and  
520 nitrogen oxidation ratio (NOR) **at** the BJ site **from** July 22-27, 2019. (e) Temporal variation **in**  
521 **the** relative humidity (RH) and temperature (T) **at** the BJ site **from** July 22-27, 2019 (the yellow  
522 mark represents the light-haze pollution period, and the red mark **represents** **the** heavy-haze  
523 pollution episode).

### 524 **3.2.1 The occurrence stage**

525 Fig. 3a **reveals** **that** the PM **level** in Beijing gradually **increased** from 8:00 to 22:00  
526 on 26 July (**the** Haze II **episode**) and from 4:00 to 22:00 on 22 July (**the** Haze I **episode**),  
527 with **the**  $\text{PM}_{2.5}$  mass **concentration** eventually reaching 75 and 131  $\mu\text{g m}^{-3}$ , respectively.  
528 **These** two stages **are** regarded as the **Haze I and Haze II** occurrence stages.

#### 529 *a. The contribution of pollution transport*

530 Owing to the **notable** control measures **in** **summer** **in** **Beijing**, the sudden elevated  
531 PM levels very likely **originated from** an outside region. **Clearly**, since the **early** hours  
532 on 22 and 26 July, Beijing was located behind the northwest-southeast trough of the  
533 850-hPa potential height field, which bordered the Sichuan Basin to the west (Fig. 7a-  
534 d; Fig. 7i-l). **Therefore**, Beijing was always **controlled by** strong southerly winds at high  
535 altitudes. With **the** Taihang **Mountains** to the east and **the** Yanshan **Mountains** to the  
536 north (Fig. 2), Beijing is **a** semi-enclosed **area**; thus, the south wind belt passing through  
537 the **North** **China** **Plain** to Beijing will be strengthened (Su et al., 2004). The southerly  
538 wind **speeds** **ranged from** 8-10  $\text{m s}^{-1}$  (**the** Haze II **period**) and **from** 5-7  $\text{m s}^{-1}$  (**the** Haze  
539 I **period**) at **altitudes**  $>0.5$  km. **Under** **persistent** **southerly** **winds**, **water** **vapor** **was**  
540 **carried to** **Beijing** **forming** **a** **moisture** **transport** **channel** **which** **increasingly** **intensified**.  
541 (Fig. 7a-d; Fig. 7i-l). In response, the humidity in Beijing **increased** in the morning of  
542 26 July with the AH (RH) **ranging from** 15-17  $\text{g m}^{-3}$  ( $\sim 75\%$ ), while **the** AH (RH)  
543 **decreased to**  $\sim 13$   $\text{g m}^{-3}$  ( $\sim 70\%$ ) from 10:00 on (Fig. 4c-d). The air temperature during



544 the daytime was extremely high, ranging from 30-35 °C (Fig. 4b), and these high-  
545 temperature weather conditions reduced the humidity by evaporation to a certain degree.  
546 Considering that the air temperature was always very high (~30 °C) since the early  
547 morning on 22 July, the AH (RH) was ~13 g m<sup>-3</sup> (~65%) during the occurrence stage.

548 With the more densely populated industrial regions located in the south of Beijing,  
549 the strong winds blowing from the south were also highly likely to transport large  
550 amounts of anthropogenic aerosols to Beijing (Chang et al., 2018; Liu et al., 2013b). To  
551 examine the potential PM transportation, we generated PM<sub>2.5</sub> mass concentration  
552 distribution maps for most parts of China (Fig. 8) and combined them with  
553 corresponding background circulation fields to elucidate the pollution transportation  
554 phenomenon. The regional distribution of the PM<sub>2.5</sub> mass concentration was obtained  
555 by interpolating PM<sub>2.5</sub> data from more than 1000 stations of the China National  
556 Environmental Monitoring Centre into a grid (0.5°×0.5°). Notably, at 2:00 on 26 and  
557 22 July, high PM<sub>2.5</sub> mass concentrations (~70 µg m<sup>-3</sup> during the Haze I episode and ~50  
558 µg m<sup>-3</sup> during the Haze II episode) mainly occurred in the south/southwest area of  
559 Beijing, which were substantially higher than that in Beijing city (~10 µg m<sup>-3</sup>) (Fig. 8a-  
560 b; Fig. 8i-l). The heavily polluted southern area of Beijing mainly included Baoding,  
561 Langfang and Shijiazhuang, which are generally 60-300 km away from Beijing (Fig.  
562 2). The southerly air mass above ~0.5 km moved faster than 20-30 km h<sup>-1</sup> (estimated  
563 from the measured wind speed) on 26 and 22 July, which was fast enough to transport  
564 pollutants to Beijing in several hours. As expected, the area with a high PM<sub>2.5</sub> mass  
565 concentration gradually spread northward corresponding to the southerly winds, and  
566 consequently, the highest PM<sub>2.5</sub> level occurred in Beijing at 20:00 on both 26 July  
567 (reaching ~65 µg m<sup>-3</sup>) and 22 July (reaching ~80 µg m<sup>-3</sup>). This was consistent with the  
568 PM<sub>2.5</sub> increase trends at this time, as shown in Fig. 3a. The average increase rate of the  
569 PM<sub>2.5</sub> concentration (~5.8 µg m<sup>-3</sup> h<sup>-1</sup>) on 22 July was higher than that on the 26 July  
570 (~3.73 µg m<sup>-3</sup> h<sup>-1</sup>), possibly related to the large difference in the PM<sub>2.5</sub> concentration  
571 between Beijing city and the southern area of Beijing. These results are consistent with  
572 the findings reported by Zhong et al. (2019). Thus, multiple results implied that PM

573 transportation by southerly winds was primarily responsible for the PM increase at the  
574 occurrence stage.

575 ***b. The effect of the atmospheric boundary layer structure***

576 As shown in Fig. 5a-b, in the mornings on 26 and 22 July, the positive values of  
577 the virtual potential temperature gradient ( $\partial\theta_v/\partial z$ ) and pseudoequivalent potential  
578 temperature gradient ( $\partial\theta_{se}/\partial z$ ) at altitudes ranging from 0-2 km (the Haze II period) and  
579 from 0-1 km altitude (the Haze I period) indicated that a stable atmosphere layer was  
580 present. Generally, with no solar radiation reaching the ground and more upward  
581 longwave radiation emitted from the ground at night, the surface cools faster than the  
582 upper atmosphere, thus promoting a stable atmosphere. In response, the turbulent  
583 kinetic energy (TKE) was extremely low ( $0-1 \text{ m}^2 \text{ s}^{-2}$ ) along with a low ABLH of  $\sim 0.5$   
584 km (Fig. 5c-d). This means that on both 26 and 22 July, south winds persisted as the  
585 ABL structure was not conducive to vertical substance diffusion. The stable ABL  
586 structure suppressing vertical pollution diffusion also contributed to the occurrence of  
587 PM pollution to a certain degree. Both  $\partial\theta_v/\partial z$  and  $\partial\theta_{se}/\partial z$  at an altitude ranging from 0-  
588 1.5 km became negative from 14:00-16:00 on 26 July, indicating an unstable  
589 atmosphere layer. Generally, the high daytime solar radiation reaching the surface may  
590 rebuild the vertical temperature structure and disrupt the stable ABL, especially in  
591 summer (Andrews, 2000). Thus, turbulence was quickly generated by the  
592 thermodynamic activity with the TKE increasing to  $2-3 \text{ s}^2 \text{ m}^{-2}$  and continuing to develop  
593 upwards, causing the ABLH to gradually increase to  $\sim 1.2$  km. This ABL process  
594 explained the slight fluctuations in the PM increase at this time in which the  $\text{PM}_{10}$  mass  
595 concentration sharply decreased from 100 to  $73 \mu\text{g m}^{-3}$ . In contrast to the ABL condition  
596 on 26 July (the Haze II stage),  $\partial\theta_{se}/\partial z$  was negative, but  $\partial\theta_v/\partial z$  was positive below  $\sim 1.5$   
597 km in the afternoon on 22 July (the Haze I stage). Combined with a low TKE ( $0-0.5 \text{ m}^2$   
598  $\text{s}^{-2}$ ) similar to that in the morning, the atmospheric stratification below  $\sim 1.5$  km  
599 remained absolutely stable. Maybe due to the low solar radiation gradually heating the  
600 ground in the afternoon under cloudy weather conditions, the original stable ABL  
601 structure previously formed in the nighttime could not be disrupted. All the above

602 results imply that the ABL structure also plays a role in the PM increase at the  
603 occurrence stage.

604 *c. Secondary aerosol formation driven by a high atmospheric oxidation capacity*

605 When the PM<sub>2.5</sub> concentration increased due to the strong southerly winds in  
606 Beijing during the Haze II (Haze I) occurrence stage, O<sub>3</sub> increased sharply, rapidly  
607 increasing from 67 (26) μg m<sup>-3</sup> and peaking at 250 (131) μg m<sup>-3</sup>. As mentioned in section  
608 3.1, a high O<sub>3</sub> concentration indicates a high atmospheric photochemical reactivity (Li  
609 et al., 2012; Seinfeld, 1986); thus, the atmosphere had a high oxidizing capacity with  
610 large amounts of free radicals (OH, etc.) and ozone, which promoted secondary aerosol  
611 formation (Pathak et al., 2009; Shi et al., 2015; Wang et al., 2016). Fig. 6b shows that  
612 along with the increase in PM<sub>2.5</sub> concentration during the occurrence stage, the organics,  
613 sulfate, and nitrate concentrations in PM<sub>2.5</sub> also gradually increased. The average  
614 organics, sulfate, and nitrate concentrations during the Haze II (Haze I) occurrence  
615 stage were 15.6 (23.0) μg m<sup>-3</sup>, 10.0 (8.0) μg m<sup>-3</sup> and 4.3 (24.7) μg m<sup>-3</sup>, respectively, and  
616 accounted for 40.7 (32.1)%, 25.3 (11.2)%, and 12.2 (31.5)%, respectively, of the PM<sub>2.5</sub>  
617 concentration. The total sulfate, organics, and nitrate (SON) concentration accounted  
618 for more than 75% of the PM<sub>2.5</sub> concentration during both the Haze II and Haze I  
619 occurrence stages (Fig. 6c), implying that the SON increase was the leading cause of  
620 the PM<sub>2.5</sub> concentration increase. Secondary organic aerosols can be formed by the  
621 photochemical oxidation reactions of the VOCs emitted by vehicles (Hennigan et al.,  
622 2011). Thus, the high concentration and relative contribution of organics are mainly  
623 attributed to the notably active photochemical reactions in summer and high VOCs  
624 emissions by vehicles in Beijing city. Due to the lack of VOCs data, the detailed  
625 formation mechanism of secondary organics will be studied in the future. To examine  
626 the possible formation mechanism of secondary inorganic aerosols, the sulfur oxidation  
627 ratio (SOR) and nitrogen oxidation ratio (NOR), defined as  $SOR = [SO_4^{2-}]/([SO_4^{2-}] + [SO_2])$  and  $NOR = [NO_3^-]/([NO_3^-] + [NO_2])$ , respectively, where [ ] indicates the  
628 molar concentration, were adopted in this paper. Higher SOR and NOR values suggest  
629 a higher oxidation efficiency of sulfur and nitrogen, which means that more secondary  
630

631 inorganic aerosols occur in the atmosphere (Liu et al., 2019c; Han et al., 2019; Yao et  
632 al., 2002; Kong et al., 2018; Sun et al., 2006).

633 Both homogeneous gas-phase and heterogeneous reactions can promote the  
634 formation of sulfate from SO<sub>2</sub> during haze episodes (Khoder, 2002; Harris et al., 2013),  
635 thereby increasing the SOR. Notably, the SOR values during the whole observation  
636 period (from 22 to 27 July) were relatively high, averaging 0.62, along with relatively  
637 low SO<sub>2</sub> levels, averaging 2.2 μg m<sup>-3</sup> (Fig. 6a; d). The observed high SOR values could  
638 be attributed to the relatively high RH (an average of ~66.6%) (Fig. 6e) and the  
639 ubiquitous photochemical reactions in summer in Beijing (Han et al., 2019).  
640 Nevertheless, compared to the very low PM level on clean days (on 25 July) (Fig. 6d),  
641 the temporal variation in the sulfate concentration on 26 July (the Haze II period) and  
642 22 July (the Haze I period) exhibited a distinct increasing trend during the occurrence  
643 stage, gradually increasing from 3.7 to 14.4 μg m<sup>-3</sup> and from 4.2 to 11.5 μg m<sup>-3</sup>,  
644 respectively. Moreover, the SOR values also averaged ~0.76 at higher levels during  
645 both the Haze II and Haze I occurrence stages compared to clean days, which attained  
646 an average of ~0.55 (Fig. 6c). The results indicated enhanced secondary sulfate aerosol  
647 formation during the occurrence stage. However, the PM level and sulfate concentration  
648 on clean days were very low, but the O<sub>3</sub> concentration was relatively high (Fig. 6a),  
649 reaching up to 214 μg m<sup>-3</sup>, which implied highly active photochemical reactions. Thus,  
650 although the notable photochemical reactions occurring during the daytime on 26 and  
651 22 July facilitated homogeneous gas-phase SO<sub>2</sub> oxidation to a certain extent, it was not  
652 the dominant reason for the sulfate increase during the occurrence stage. Notably, the  
653 PM level and total chemical component mass concentration slowly increased on 24 July  
654 with no pollution transportation by south winds (Fig. 3a-b; Fig. 7e-h; Fig. 8e-h;), while  
655 the average sulfate concentration was 2.8 μg m<sup>-3</sup> and only accounted for 10.7% of the  
656 PM<sub>2.5</sub> concentration, far lower than that during the Haze II period and similar to that on  
657 clean days. The average RH was 61.4% and 75.3% during the Haze II and Haze I  
658 occurrence stages, respectively, which was also higher than that on clean days (54.5%).  
659 According to the results mentioned above, the strong winds blowing from the south and

660 southwest of Beijing transport much moisture and particles, and we infer that the  
661 increase in sulfate aerosols during the Haze II and Haze I periods can be mainly  
662 attributed to regional transport. Hence, the moisture and particles transported to Beijing  
663 further facilitated the heterogeneous reactions of SO<sub>2</sub> on the moist aerosol surface. This  
664 highlights the importance and urgency of enhancing joint regional pollution emission  
665 control.

666 Nitrate is predominantly formed via both the homogeneous gas-phase  
667 photochemical reaction of NO<sub>2</sub> with OH radicals in the daytime when the  
668 photochemical activity is high (Wang et al., 2006; Wen et al., 2018; Seinfeld and Pandis,  
669 2006) and the heterogeneous hydrolysis reaction of NO<sub>3</sub> and N<sub>2</sub>O<sub>5</sub> in the atmosphere in  
670 the nighttime (Richards, 1983; Russell et al., 1986; Wang et al., 2009; Wang et al.,  
671 2017a; Pathak et al., 2011). In addition, there exists an equilibrium between particulate  
672 nitrate and gaseous HNO<sub>3</sub> and NH<sub>3</sub> in the atmosphere because ammonium nitrate is  
673 semi-volatile (Seinfeld, 1986). A high temperature could promote ammonium nitrate  
674 decomposition; thus, the regional transport of ammonium nitrate in summer was not  
675 considered (Li et al., 2019). Fig. 6b and d reveal that the nitrate concentration (NOR)  
676 during the occurrence Haze II stage slightly increased from 3.2 μg m<sup>-3</sup> (0.09) at 8:00 to  
677 5.2 μg m<sup>-3</sup> (0.23) at 22:00. The nitrate concentration (NOR) during the Haze I  
678 occurrence stage sharply increased from 2.7 μg m<sup>-3</sup> (0.02) at 8:00 to 38.1 μg m<sup>-3</sup> (0.36)  
679 at 16:00. The nitrate concentration and relative contribution to PM during the Haze I  
680 period were markedly higher than those during the Haze II period (Fig. 6c). This  
681 inconsistency could be attributed to the higher temperature (averaging ~34 °C) during  
682 the Haze II period than that during the Haze I period (averaging ~27 °C) (Fig. 6e). These  
683 results indicated that strong photochemical reactions facilitated nitrate formation,  
684 thereby increasing the PM<sub>2.5</sub> level, while nitrate decomposed into gaseous HNO<sub>3</sub> and  
685 NH<sub>3</sub> once the temperature was high enough. After 15:00, the nitrate concentration  
686 increased in the presence of large amounts of radicals, and the temperature drop  
687 inhibited the reverse reaction. In the nighttime, the increase in nitrate aerosols was  
688 predominantly attributed to the heterogeneous hydrolysis reactions of NO<sub>3</sub> and N<sub>2</sub>O<sub>5</sub> in

689 the atmosphere; more details are provided in the next section.

### 690 3.2.2 The outbreak stage

691 The PM<sub>2.5</sub> mass concentration suddenly increased from 75  $\mu\text{g m}^{-3}$  at 22:00 on 26  
692 July to 146  $\mu\text{g m}^{-3}$  at 4:00 on 27 July and remained high at  $\sim 150 \mu\text{g m}^{-3}$  until 10:00,  
693 which was identified as the outbreak stage of haze pollution (Fig. 3a). Compared to  
694 the atmospheric BSC ranging from 2.5-3  $\text{M m}^{-1} \text{sr}^{-1}$  on 26 July, the ambient particle  
695 concentration below the  $\sim 0.5$ -km altitude sharply increased the atmospheric scattering  
696 coefficient, exceeding 6  $\text{M m}^{-1} \text{sr}^{-1}$  (Fig. 3b).

#### 697 a. The almost negligible contribution of southerly transport

698 There were still strong southerly winds controlling Beijing at high altitudes ( $>0.5$   
699 km), accompanied by a more notable vapor transportation channel below (Fig. 7m-n).  
700 However, the PM levels in the south/southeast area of Beijing, ranging from 0 to  $\sim 60$   
701  $\mu\text{g m}^{-3}$ , were significantly lower than those ( $>80 \mu\text{g m}^{-3}$ ) in Beijing, even below air  
702 quality standards (Fig. 8n-m). It was unlikely that the explosive PM growth and the  
703 persistent high PM level in Beijing were caused by pollution transportation.

#### 704 b. Extremely stable ABL structures are a prerequisite for pollution outbreaks

705 Without pollution transportation, more attention was focused on the interior of  
706 the local ABL, and Fig. 5 shows the temporal variation in the ABL structure. Both the  
707  $\partial\theta_v/\partial z$  and  $\partial\theta_{se}/\partial z$  values became positive ( $\sim 1.5 \text{ }^\circ\text{C}/100 \text{ m}$  and  $\sim 2.5 \text{ }^\circ\text{C}/100 \text{ m}$ ,  
708 respectively) below the  $\sim 0.3$ -km altitude, as depicted in Fig. 5a-b. This implied that a  
709 very stable lower layer defined as the nocturnal stable boundary layer (NSBL) had  
710 formed with an ABLH of  $\sim 0.3$  km. Due to the notable radiation effect of the already  
711 high aerosol loading during the daytime, the surface solar radiation was greatly  
712 blocked and reduced, which promoted stable stratification at midnight (Zhao et al.,  
713 2019; Zhong et al., 2017). In such a thermally stable state, the buoyancy transport heat  
714 flux in the atmosphere continuously consumes turbulent energy, suppressing the  
715 development of turbulence. Therefore, the corresponding TKE had sharply decreased  
716 compared to that from 14:00-16:00 on 26 July, lower than  $\sim 0.5 \text{ m}^2 \text{ s}^{-2}$  and even  
717 approaching  $\sim 0 \text{ m}^2 \text{ s}^{-2}$  (Fig. 5c-d). However, the  $\partial\theta_v/\partial z$  and  $\partial\theta_{se}/\partial z$  values were positive

718 and negative, respectively, from ~0.3 to ~1.5 km, which implies that this atmospheric  
719 layer was conditionally unstable. Considering the very low TKE like that below ~0.3  
720 km, this layer, referred to as the residual layer, was also absolutely stable. Thus, the  
721 ambient particles were restrained from vertically spreading and were concentrated  
722 below the NSBL, thereby increasing the ground PM level. Similarly, ambient water  
723 vapor was also not conducive to dispersed, which explained the extremely high  
724 humidity during this period. As shown in Fig. 4c-d, the atmospheric humidity during  
725 the outbreak stage was distinctly higher than that on 26 July with the AH (RH) reaching  
726 ~20 g m<sup>-3</sup> (~90%). In contrast to the role of the moisture transport channel, the unique  
727 NSBL structure has a more notable impact on the increase in air humidity.

728 In contrast, during the Haze I period on 22 July, no PM pollution outbreak stage  
729 occurred, as the PM<sub>2.5</sub> mass concentration had sharply decreased from 131 to 53 μg  
730 m<sup>-3</sup> in one hour since 21:00. The ambient particles did not accumulate and maintained  
731 a high level, similar to that during the Haze II period, because the ABL structure did  
732 not exhibit similar characteristics. The already high PM<sub>2.5</sub> level (~130 μg m<sup>-3</sup>) in the  
733 daytime accelerated surface cooling, causing the NSBL to more readily form at a very  
734 low height of ~0.2 km. This situation was similar to that during the Haze II episode.  
735 Nevertheless, the TKE above the NSBL was very high, reaching 2-3 m<sup>2</sup> s<sup>-2</sup>, in notable  
736 contrast to that during the Haze II episode, where the TKE was extremely low (~0 m<sup>2</sup>  
737 s<sup>-2</sup>) across the whole 0-1.5 km layer. The vertical temperature structures above the  
738 NSBL indicated that the atmosphere had attained conditional instability, while in terms  
739 of the TKE distribution, the atmospheric stratification above the NSBL during the  
740 Haze I period was unstable, in contrast to the stable stratification during the Haze II  
741 period. Because it rained at night with a high AH (15-20 g m<sup>-3</sup>) and RH (>90%)  
742 extending from the surface up to an altitude of ~3 km, the convection activity was  
743 quite strong accompanied by a wet deposition process. Due to the unstable ABL  
744 structure and the accompanying wet deposition, the ambient particle concentration did  
745 not sharply increase, but particles were instead removed from the atmosphere.

746 Noted that the PM level on 24 July also tended to increase, but it suddenly

747 decreased, similar to that during the Haze I stage. There was no transportation effect  
748 contributing to the increase in PM level on 24 July under westerly circulation field  
749 control (Fig. 7e-h). Similar to the Haze I and Haze II occurrence stages, a stable  
750 atmosphere near the surface had formed with positive  $\partial\theta_v/\partial z$  and  $\partial\theta_{sc}/\partial z$  values. Under  
751 this stable stratification, the PM from local emissions started increasing on 24 July. The  
752 anomalous vertical temperature structures during the nighttime were disrupted and  
753 transformed into unstable stratifications at the daytime, with negative  $\partial\theta_{sc}/\partial z$  ( $\partial\theta_v/\partial z$ )  
754 profiles. As observed during the Haze II episode, the ABL structure characterized by an  
755 increased TKE ( $2\text{-}3\text{ m}^2\text{ s}^{-2}$ ) and elevated ABLH ( $\sim 1.5\text{ km}$ ) resulted in rapid pollution  
756 dissipation. However, the difference between the Haze II process and the pollution  
757 process on 24 July was that the unstable atmospheric stratification with a high TKE on  
758 24 July continued to develop until the end of the day, while for the Haze II process, this  
759 condition lasted only two or three hours at noon. Additionally, an NSBL was established  
760 at midnight during the Haze II process at an ABLH of  $\sim 0.3\text{ km}$ , thus worsening the  
761 near-stratum vertical diffusion conditions. Therefore, the subsequent stable atmospheric  
762 stratification on 26 July was a prerequisite for the pollution outbreak during the Haze  
763 II process. Particles would not accumulate and cause pollution outbreak without a stable  
764 ABL structure but were easily removed by the self-cleaning capacity of the atmosphere.

765 *c. Intense secondary aerosol formation driven by the atmospheric oxidation*  
766 *capacity causing the pollution outbreak*

767 Heterogeneous aqueous reactions refer to the secondary formation of sulfates and  
768 nitrates largely related to the ambient humidity (Wang et al., 2012). The accumulation  
769 of water vapor in the NSBL facilitated secondary aerosol formation and further  
770 promoted the outbreak of PM pollution. To investigate the explosive growth  
771 mechanisms, we divided the PM pollution outbreak stage during the Haze II process  
772 into two stages: stage I, from 22:00 on 26 July to 4:00 on 27 July; stage II, from 5:00 to  
773 10:00 on 27 July. During stage I, along with the explosive growth in  $\text{PM}_{2.5}$ , the nitrate  
774 concentration rapidly increased from  $11.6$  to  $57.8\text{ }\mu\text{g m}^{-3}$ , while sulfate and organics  
775 slightly increased from  $13.7$  to  $19.8\text{ }\mu\text{g m}^{-3}$  and from  $21.8$  to  $24.9\text{ }\mu\text{g m}^{-3}$ , respectively



776 (Fig. 6d). During stage II, the nitrate concentration remained at its highest level of ~57  
777  $\mu\text{g m}^{-3}$ , and the sulfate level remained at ~19  $\mu\text{g m}^{-3}$ , with the organics slowly  
778 decreasing (Fig. 6d). The explosive growth trend of nitrate is the most consistent with  
779 that of  $\text{PM}_{2.5}$ . In addition, the average organics, sulfate, and nitrate concentrations  
780 during the whole outbreak stage were 20.6, 15.9 and 43.0  $\mu\text{g m}^{-3}$ , respectively, and  
781 accounted for 22.0%, 17.8%, 34.9%, respectively, of the  $\text{PM}_{2.5}$  concentration.  
782 Compared to the occurrence stage, the relative contributions of organics and sulfate to  
783  $\text{PM}_{2.5}$  decreased significantly, while the contribution of nitrate notably increased. These  
784 results indicated that the explosive  $\text{PM}_{2.5}$  concentration growth was driven by the sharp  
785 increase in nitrate concentration. With strong photochemical reactions during the  
786 daytime, the  $\text{O}_3$  mass concentration was very high before the outbreak stage, up to 214  
787  $\mu\text{g m}^{-3}$ .  $\text{NO}_2$  was produced by  $\text{O}_3$  reacting with a large amount of  $\text{NO}$ , which was  
788 discharged by vehicles during evening hours.  $\text{NO}_2$  reacted with  $\text{O}_3$  aloft to form  $\text{NO}_3$ ,  
789 which rapidly reacted with  $\text{NO}_2$  to form  $\text{N}_2\text{O}_5$  at night. During stage I, NOR rapidly  
790 increased from 0.26 to 0.60, which implied that the  $\text{NO}_2$  oxidization rate sharply  
791 increased within a few hours. Considering that  $\text{NO}_2$  remained relatively low at ~25  $\mu\text{g m}^{-3}$   
792 and  $\text{O}_3$  rapidly decreased from 214 to 46  $\mu\text{g m}^{-3}$  during stage I (Fig. 6a), the  
793 consumption process of  $\text{NO}_2$  was more significant than its generation process. The  $\text{NO}_2$   
794 produced through  $\text{O}_3$  consumption was constantly oxidized by  $\text{O}_3$  to generate a large  
795 amount of  $\text{N}_2\text{O}_5$ , resulting in a sharp decline in the  $\text{O}_3$  concentration. Once  $\text{N}_2\text{O}_5$  was  
796 produced, it would be adsorbed onto moist particle surfaces and react with water  
797 droplets to form nitrate, resulting in a sudden nitrate increase, from 11.6 to 57.8  $\mu\text{g m}^{-3}$ .  
798 During stage II,  $\text{O}_3$  slowly decreased to 34  $\mu\text{g m}^{-3}$  at 6:00 on 27 July, and  $\text{NO}_2$   
799 remained relatively high (44-51  $\mu\text{g m}^{-3}$ ), which meant that the  $\text{NO}_2$  generation process  
800 dominated. Thus, the oxidization of  $\text{NO}_2$  did not further increase as the NOR remained  
801 at ~0.45 during stage II. Hence, nitrate, formed along the pathway whereby  $\text{N}_2\text{O}_5$  was  
802 adsorbed onto surfaces and reacted with water droplets, did not further increase,  
803 maintaining its highest mass concentration of ~57  $\mu\text{g m}^{-3}$ . The processes mentioned  
804 above were unimportant during the daytime because  $\text{N}_2\text{O}_5$  was in equilibrium with  $\text{NO}_3$ ;

805 that is, NO<sub>3</sub> was photolyzed and rapidly destroyed by NO, which in turn occurred  
806 whenever NO<sub>x</sub> and sunlight were present. During both stages I and II, the SOR always  
807 remained relatively high at ~0.95, accompanied by a high RH of ~90%. A high SOR  
808 and RH signified that heterogeneous reactions dominated the formation of particulate  
809 sulfate during the outbreak stage. The increased sulfate amount, which was lower than  
810 that of nitrate, may be related to the low SO<sub>2</sub> emissions and massive NO emissions from  
811 the large number of vehicles. This highlights the importance and urgency of enhancing  
812 NO<sub>x</sub> (vehicle) emission control.

813 Contrary to expectations, after the wet deposition process during the Haze I period,  
814 the PM<sub>2.5</sub> and NO<sub>2</sub> concentrations and the total chemical composition abruptly  
815 increased at 0:00 on 23 July, accompanied by a sharp increase in nitrate and NOR (from  
816 9.3 to 41.5 μg m<sup>-3</sup> and from 0.26 to 0.49, respectively). These results may be related to  
817 the high RH (higher than 93%), which facilitated the heterogeneous hydrolysis reaction  
818 of NO<sub>3</sub> and N<sub>2</sub>O<sub>5</sub>, formed from gas pollutants NO<sub>x</sub> and O<sub>3</sub> not completely removed in  
819 the wet deposition process.

### 820 3.2.3 The diffusion stage

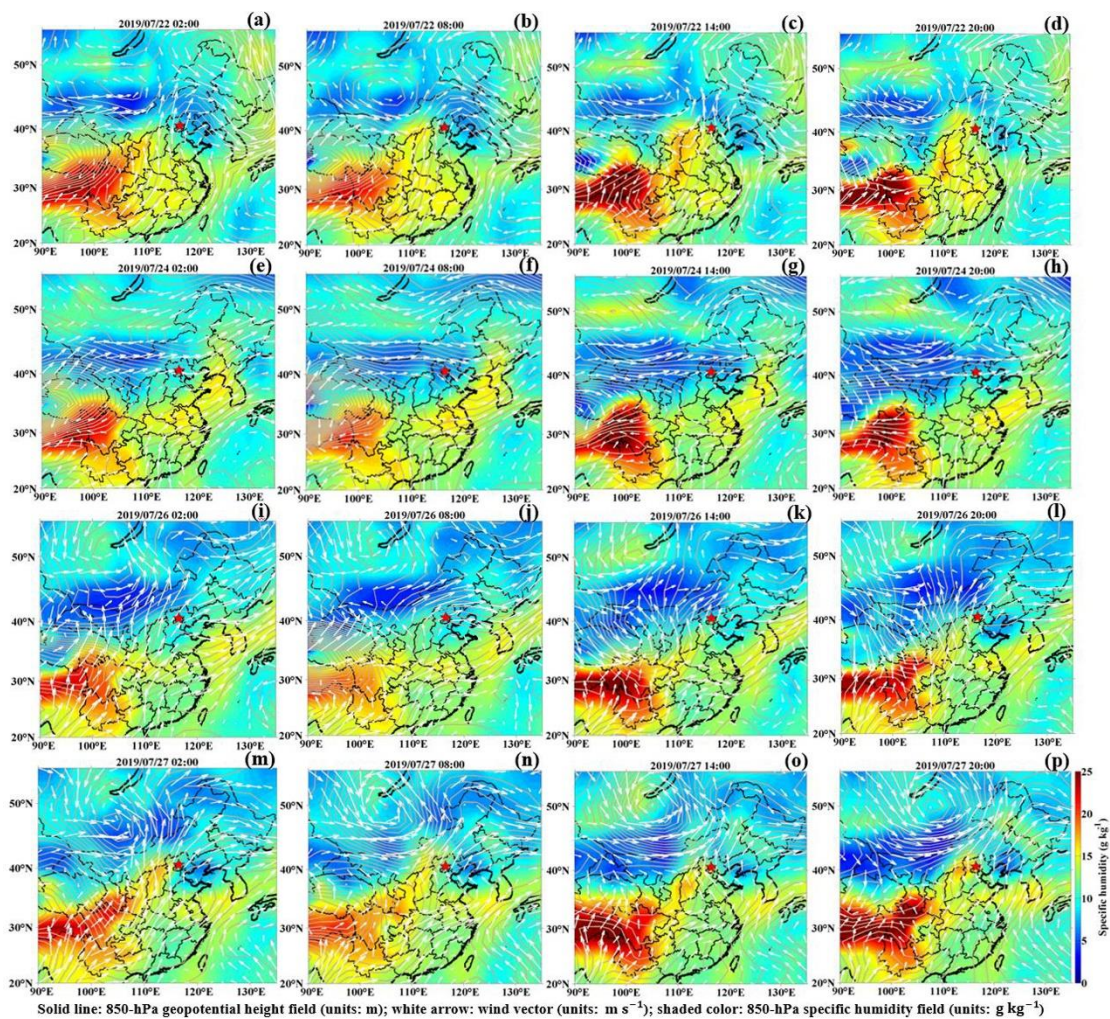
821 After 10:00 on 27 July, the PM<sub>2.5</sub> mass concentration sharply decreased to 50 μg  
822 m<sup>-3</sup> over three hours, during which the atmospheric BSC decreased to <1×10<sup>3</sup> M m<sup>-1</sup> sr<sup>-1</sup>  
823 across the whole ABL (Fig. 3 and Fig. 8o-p). This represented the pollution diffusion  
824 stage. As no wet deposition process occurred, the Haze II diffusion stage was different  
825 from that of Haze I. Generally, the arrival of strong and clean air masses from the south  
826 is the main factor dissipating air pollution in Beijing (Zhong et al., 2017; Zhong et al.,  
827 2018; Zhao et al., 2019). Calm/light winds in the lower layer dominated during the  
828 outbreak stage, while sudden increased southeast winds persisted in the 0-2 km layer  
829 after 8:00 on 27 July, with a wind speed of 6-9 m s<sup>-1</sup> (Fig. 7n-q and Fig. 4a). The  
830 southeast winds originated from the Bohai Sea and the Yellow Sea. Moreover, during  
831 this diffusion stage, the air quality of the southeast of Beijing was basically clean or  
832 much better than that in Beijing (Figure 8(n)-(p)). Therefore, strong southeast winds  
833 would not bring pollutants aggravating the pollution in Beijing instead played a role in

834 the horizontal diffusion of the accumulated PM at the surface. On the other hand,  
835 accompanied by the horizontal diffusion, the strong solar radiation at noon reached the  
836 surface and changed the vertical temperature structure. The ABL was extremely  
837 unstable in terms of both  $\partial\theta_v/\partial z$  and  $\partial\theta_{se}/\partial z$ , which were negative below  $\sim 1.0$  km with  
838 values of  $-0.5$  °C/100 m and  $-2.5$  °C/100 m, respectively (Fig. 5a-b). Along with this  
839 instability, the development of turbulence in the ABL was very strong and quick, with  
840 the TKE suddenly increasing to  $3-5$   $\text{m}^2 \text{s}^{-2}$  (Fig. 5c). Accompanied by pronounced  
841 turbulence development, the ABL continuously developed upward with the ABLH up  
842 to  $\sim 2.5$  km over a short time (Fig. 5d). The ABL structure quickly became extremely  
843 suitable for vertical pollutant diffusion; thus, the PM level sharply decreased during this  
844 time.

845 In contrast to  $\text{PM}_{2.5}$ , the  $\text{O}_3$  concentration rapidly increased with increasing  
846 radiation, along with the high  $\text{NO}_2$  and  $\text{NO}$  concentrations attributed to morning traffic  
847 emissions. Along with the decline in  $\text{PM}_{2.5}$ , organics and sulfate slowly decreased to  
848 below  $\sim 3$   $\mu\text{g m}^{-3}$ , and nitrate decreased to below  $1.0$   $\mu\text{g m}^{-3}$ . The average organics,  
849 sulfate, and nitrate concentrations were as low as 6.8, 6.2 and  $1.9$   $\mu\text{g m}^{-3}$ , respectively,  
850 and accounted for 33.0%, 32.3%, and 6.0%, respectively, of the  $\text{PM}_{2.5}$  concentration.  
851 As the significant turbulence activity caused vertical transportation of vapor, heat, and  
852 particles, the RH decreased to  $\sim 60\%$ , accompanied by a decline in SOR ( $\sim 0.75$ ). This  
853 emphasized the notable correlation between the humidity and the heterogeneous  
854 formation mechanism of sulfate. In addition, the NOR rapidly decreased from 0.22 to  
855 0.01, coinciding with the change in nitrate. At this stage, the temperature always  
856 remained high at  $\sim 35$  °C. Thus, similar to the occurrence stage, ammonium nitrate  
857 evaporated at high temperatures, contributing to a decline in nitrate. In summary, during  
858 the diffusion stage, the unstable ABL structure was not only conducive to pollution  
859 diffusion but also affected T and RH to inhibit secondary aerosol formation and further  
860 reduced secondary aerosols.

861 Regardless of the wet deposition process during the Haze I period or the horizontal  
862 and vertical diffusion during the Haze II period, air pollution eventually dissipated as

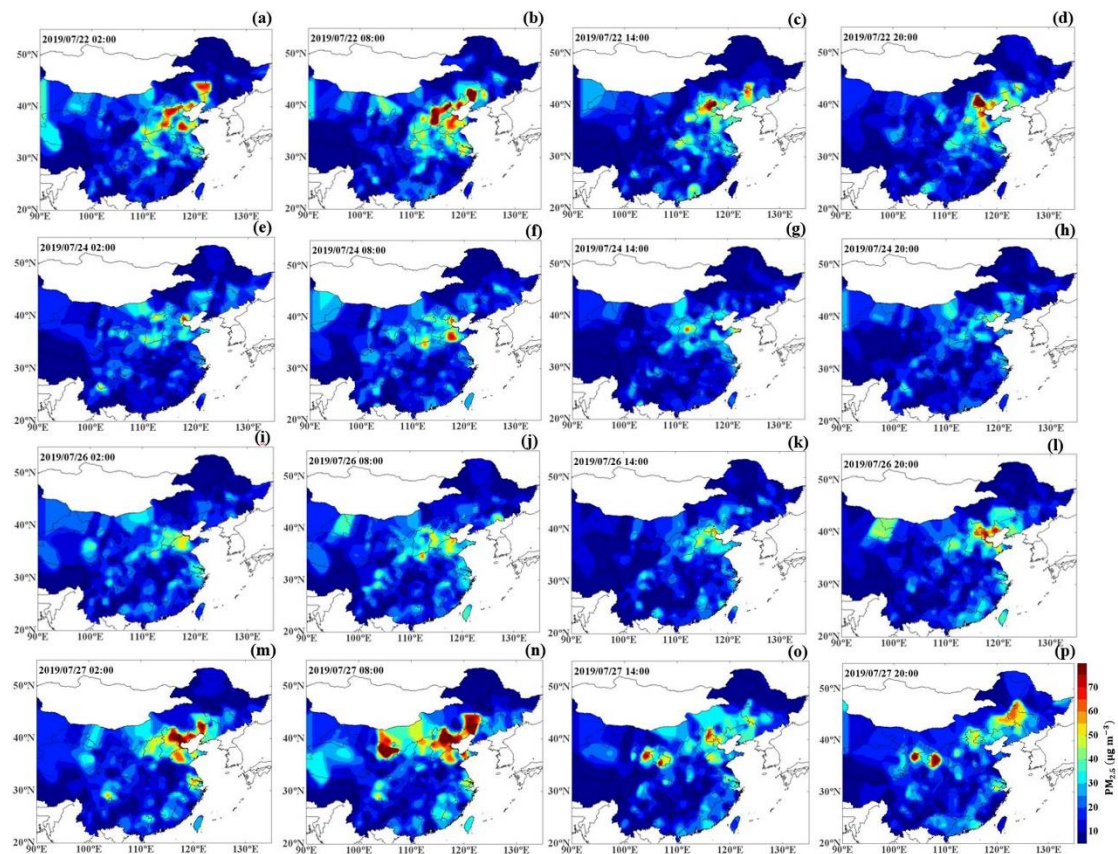
863 long as the atmosphere **was in** a specific state. In other words, **this** implies that the self-  
 864 cleaning capacity of the atmosphere **was** responsible for air pollution **dispersion**. When  
 865 the atmosphere **attains a specific** state, **its** self-cleaning capacity **removes** pollution. To  
 866 **examine this phenomenon**, the key factors characterizing the self-cleaning capacity of  
 867 the atmosphere should be **determined** first. As analyzed above, once the TKE increased  
 868 to  $>1.5\text{-}2\text{ m}^2\text{ s}^{-2}$ , the ABLH **increased and exceeded**  $\sim 1\text{ km}$ , and the  $\partial\theta_v/\partial z$  **and**  $\partial\theta_{sc}/\partial z$   
 869 **values became** negative, as well as no calm/light winds **persisted**. The atmosphere was  
 870 **unstable** with **notable** turbulence activities and advection transport, and air pollution was  
 871 **immediately dissipated**. Owing to **the** limited observation time, the results **regarding**  
 872 the characteristics of **the** self-cleaning capacity of the atmosphere may **not** be universal,  
 873 and **a** more comprehensive **investigation** on the self-cleaning capacity of the atmosphere  
 874 **will be conducted** in the future.



875

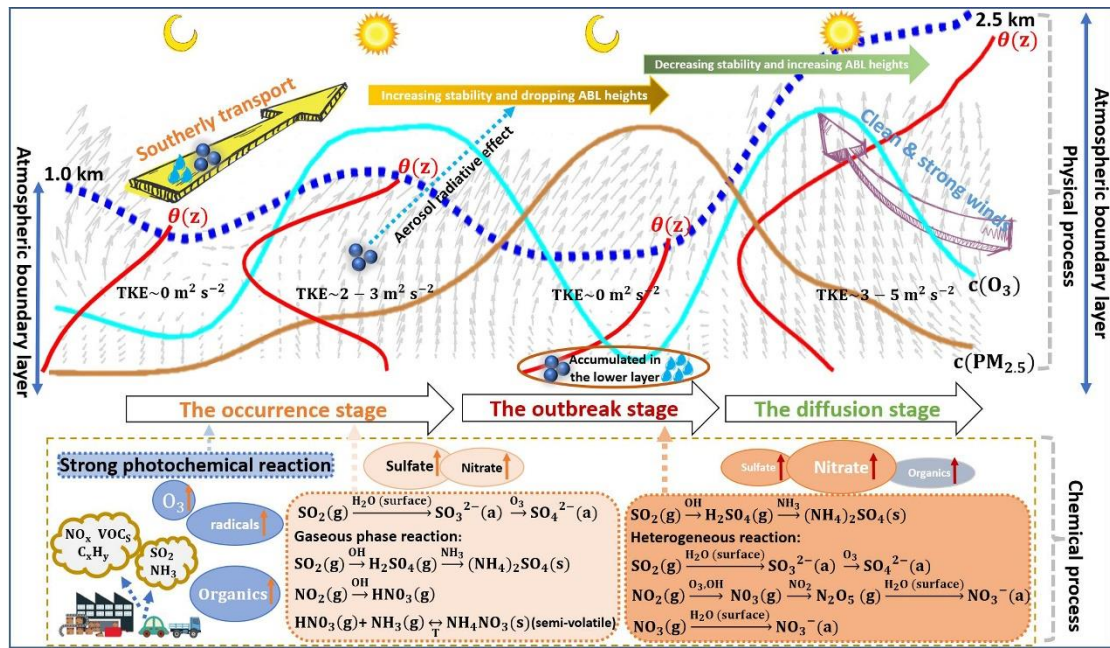
876 **Figure 7. Composites of the 850-hPa horizontal wind vector field (units:  $\text{m s}^{-1}$ ; white arrows),**

877 850-hPa geopotential height field (units: m; solid lines) and 850-hPa specific humidity field  
 878 (units:  $\text{g kg}^{-1}$ ; shaded colors) at 0200, 0800, 1400, and 2000 (local time) on 22 and 24 July and  
 879 from 26-27 July, labeled as (a) - (p). The star shows the location of the BJ site.  
 880



881  
 882 Figure 8. The  $\text{PM}_{2.5}$  mass concentration distribution (units:  $\mu\text{g m}^{-3}$ ; shaded colors) over most of  
 883 China at 0200, 0800, 1400, and 2000 (local time) on 22 and 24 July and from 26–27 July,  
 884 labeled as (a)–(p).

885 **4 Conclusion**



886

887 Figure 9. Schematic diagram for the formation mechanism of haze pollution under a high  
 888 atmospheric oxidization capacity in summer in Beijing (blue dashed line: atmospheric  
 889 boundary layer; red solid lines: potential temperature gradient profiles; brown solid line:  
 890 temporal change curve of the ozone concentration; cyan solid line: temporal change curve of  
 891 the PM<sub>2.5</sub> mass concentration; gray arrow sectors: temporal change in the wind vector profiles;  
 892 TKE: turbulence kinetic energy; solid dots: particulate matter in the atmosphere; droplets: water  
 893 vapor).

894 The extremely serious haze pollution episode characterized by  
 895 alternating/synchronous heavy PM loadings and high ozone concentrations occurred  
 896 this summer in Beijing. Combined with a series of observations, the formation  
 897 mechanism of haze pollution under a high atmospheric oxidization capacity has been  
 898 systematically analyzed in terms of the atmospheric physical and chemical processes  
 899 and schematically depicted in Fig. 9. The occurrence of haze pollution in summer in  
 900 Beijing was mainly attributed to southerly transport and influenced by the ABL  
 901 structure to a certain degree (physical process), which was further promoted by intense  
 902 secondary aerosol formation under a high atmospheric oxidation capacity (chemical  
 903 process). On the one hand, the physical process, where large amounts of moisture and  
 904 particles were transported to Beijing by strong southerly winds, caused haze pollution  
 905 initiation in Beijing, consistent with previous studies, e.g., Huang et al. (2017) and

906 Zhong et al. (2019). Moreover, we found that haze pollution occurred when the ABL  
907 structure was extremely stable with a low TKE and a positive potential temperature  
908 gradient ( $\partial\theta/\partial z$ ), which increased the PM level in Beijing. The stable ABL was  
909 disrupted and transformed into an unstable structure (negative  $\partial\theta/\partial z$ ) with high solar  
910 radiation in the afternoon (Andrews, 2000), responsible for the fluctuations in the PM  
911 increase process. On the other hand, the concentration of secondary aerosols such as  
912 sulfate, nitrate, and organics quickly increased. The very high O<sub>3</sub> concentration in the  
913 daytime indicates an active atmospheric photochemical reactivity (Li et al., 2012;  
914 Seinfeld, 1986) and a high atmospheric oxidizing capacity with large amounts of free  
915 radicals (OH, etc.) and ozone, which promotes secondary aerosol formation (Pathak et  
916 al., 2009; Shi et al., 2015; Wang et al., 2016). However, we found that the distinct  
917 increase in sulfate concentration was mainly linked to southerly transport, which carried  
918 heavy sulfate aerosol loadings to Beijing. The physical process, where the extremely  
919 stable ABL inhibited PM and moisture diffusion, thus increasing the ambient humidity  
920 and ground-level PM<sub>2.5</sub>, was a prerequisite for haze pollution outbreak. Under a stable  
921 ABL, secondary aerosol formation dominated by nitrate was quite intense, driving the  
922 pollution outbreak. The PM levels in the south/southeast area of Beijing were  
923 significantly lower than those in Beijing, even below air quality standards. The  
924 contribution of pollution transport was negligible. Owing to the already high PM<sub>2.5</sub> level  
925 during the daytime, the strong aerosol radiation effect cooled the surface and heated the  
926 above layer (Dickerson et al., 1997; Stone et al., 2008; Wilcox et al., 2016), which  
927 facilitated NSBL formation. The  $\partial\theta/\partial z$  value in the NSBL was thus found to be positive,  
928 thus increasing the atmospheric stability, decreasing the ABLH and decreasing the TKE.  
929 The ambient particles and moisture would be restrained from vertically spreading and  
930 became concentrated below the NSBL (Stone et al., 2008), resulting in elevated PM  
931 and humidity levels at the surface. In addition, there was a large increase in NOR and  
932 an explosive growth in the nitrate concentration during the outbreak stage. Due to the  
933 high O<sub>3</sub> level produced by the intense photochemical reactions during the daytime and  
934 the NO<sub>x</sub> discharged by vehicles during evening peak hours, vast amounts of N<sub>2</sub>O<sub>5</sub> and

935 NO<sub>3</sub> were formed through oxidization reactions (Chang et al., 1967; Wilson Jr et al.,  
936 1972). Under a very high humidity, the heterogeneous hydrolysis reactions of N<sub>2</sub>O<sub>5</sub> and  
937 NO<sub>3</sub> at the moist particle surface were very notable, resulting in the formation of large  
938 amounts of nitrate aerosols (Richards, 1983; Russell et al., 1986; Wang et al., 2009;  
939 Wang et al., 2017a; Pathak et al., 2011). Considering that pollutant transport from  
940 outside considerably affected haze formation in Beijing, especially during the  
941 occurrence stage, continuous regional joint control of air pollution should be enhanced.  
942 In addition, as reported in previous studies (Li et al., 2012; Pathak et al., 2009; Seinfeld,  
943 1986; Shi et al., 2015; Wang et al., 2016; Zhong et al., 2018) and confirmed in this study,  
944 the atmospheric oxidization capacity, enhanced by photochemical reactions, largely  
945 facilitated secondary aerosol formation, which further aggravated pollution. In this  
946 study, secondary organic aerosols and secondary nitrate aerosols significantly increased  
947 and were the most important constituents of particles during the haze episodes.  
948 Photolysis of NO<sub>x</sub> triggers photochemical reactions, in which the reactions with VOCs  
949 are important (Hennigan et al., 2011; Seinfeld and Pandis, 2006; Wang et al., 2006; Wen  
950 et al., 2018). Additionally, NO<sub>x</sub> and VOCs are precursors of nitrate and organics,  
951 respectively. Thus, controls should be strengthened for supervising heavy diesel  
952 vehicles and collaboratively controlling NO<sub>x</sub> and VOC emissions. As the PM level  
953 gradually increased, a wet deposition process and an extremely unstable ABL structure  
954 were observed on 22 July (the Haze I period) and 24 July, respectively, and the ambient  
955 particles sharply decreased before the outbreak stage. This emphasized that the ABL  
956 structure extremely restrained the diffusion of substances and was a prerequisite for  
957 pollution outbreaks. With clean and strong winds passing through Beijing, the ABL  
958 became unstable with a negative  $\partial\theta/\partial z$  value and an increased ABLH. The high  
959 turbulence activity promoted pollution diffusion. Regardless of the wet deposition  
960 process or the high turbulence activity, air pollution would eventually dissipate once  
961 the atmosphere was in a specific state. The self-cleaning capacity of the atmosphere  
962 was responsible for air pollution diffusion. When the atmosphere is in a specific state,  
963 its self-cleaning capacity becomes dominant, which is worthy of further study.



964 **Data availability**

965 The surface PM<sub>2.5</sub> and PM<sub>10</sub> data and observation data of the other trace gases in this  
966 study can be accessed at <http://106.37.208.233:20035/>. Atmospheric reanalysis data  
967 were obtained from the National Centers for Environmental Prediction (NCEP)  
968 (<https://www.esrl.noaa.gov/psd/data/>). The other datasets can be obtained upon request  
969 from the corresponding author.

970 **Author contribution**

971 ZD and LG performed the research and wrote the paper, contributing equally to this  
972 study. XJ, QJ, WY and WX provided writing guidance, revised and polished the paper.  
973 LZ, TG, HB and WL designed the experiments and DL, MY, WX and WF carried them  
974 out. GC contributed to discussions of results. All the authors have made substantial  
975 contributions to the work reported in the manuscript.

976 **Competing interests.**

977 The authors declare that they have no conflict of interest.

978 **Acknowledgments**

979 This study was supported by the Ministry of Science and Technology of China  
980 (grant number 2016YFC0202001), the CAS Strategic Priority Research Program  
981 (XDA23020301) and the National Natural Science Foundation of China (grant number  
982 41375036). The authors are grateful for services rendered by the National Oceanic and  
983 Atmospheric Administration (NOAA) and National Centers for Environmental  
984 Prediction (NCEP). The authors are thankful for the data support from the National  
985 Earth System Science Data Sharing Infrastructure, National Science & Technology  
986 Infrastructure of China (available at <http://www.geodata.cn>).

987 **References**

988 Andrews, D. G.: An Introduction to Atmospheric Physics, Cambridge University Press,  
989 <https://doi.org/10.1017/CBO9780511800788>, 2000.

990 Ainsworth, E. A., Yendrek, C. R., Sitch, S., Collins, W. J., and Emberson, L. D.: The effects of  
991 tropospheric ozone on net primary productivity and implications for climate change, *Annu. Rev. Plant*  
992 *Biol.*, 63, 637-661, <https://doi.org/10.1146/annurev-arplant-042110-103829>, 2012.

993 Anger, A., Dessens, O., Xi, F., Barker, T., and Wu, R.: China's air pollution reduction efforts may result  
994 in an increase in surface ozone levels in highly polluted areas, *Ambio*, 45, 254-265,  
995 <https://doi.org/10.1007/s13280-015-0700-6>, 2016.

996 Banta, R. M., Pichugina, Y. L., and Brewer, W. A.: Turbulent velocity-variance profiles in the stable  
997 boundary layer generated by a nocturnal low-level jet, *J. Atmos. Sci.*, 63, 2700-2719,  
998 <https://doi.org/10.1175/jas3776.1>, 2006.

999 Bi, J., Huang, J., Shi, J., Hu, Z., Zhou, T., Zhang, G., Huang, Z., Wang, X., and Jin, H.: Measurement of  
1000 scattering and absorption properties of dust aerosol in a Gobi farmland region of northwestern China - a  
1001 potential anthropogenic influence, *Atmos. Chem. Phys.*, 17, 7775-7792, [https://doi.org/10.5194/acp-17-](https://doi.org/10.5194/acp-17-7775-2017)  
1002 [7775-2017](https://doi.org/10.5194/acp-17-7775-2017), 2017.

1003 **Chang, T.Y., Kuntasal, G., Pierson, W.R.: Night-time N2O5/NO3 chemistry and nitrate in dew water,**  
1004 ***Atmos. Environ.*, 21(6), 1345-1351, [https://doi.org/10.1016/0004-6981\(67\)90081-9](https://doi.org/10.1016/0004-6981(67)90081-9), 1967.**

1005 Chang, X., Wang, S., Zhao, B., Cai, S., and Hao, J.: Assessment of inter-city transport of particulate  
1006 matter in the Beijing-Tianjin-Hebei region, *Atmos. Chem. Phys.*, 18, 4843-4858,  
1007 <https://doi.org/10.5194/acp-18-4843-2018>, 2018.

1008 Chen, L., Guo, B., Huang, J., He, J., Wang, H., Zhang, S., and Chen, S. X.: Assessing air-quality in  
1009 Beijing-Tianjin-Hebei region: The method and mixed tales of PM<sub>2.5</sub> and O<sub>3</sub>, *Atmos. Environ.*, 193,  
1010 290-301, <https://doi.org/10.1016/j.atmosenv.2018.08.047>, 2018.

1011 Chen, Z., Chen, D., Wen, W., Zhuang, Y., Kwan, M. P., Chen, B., Zhao, B., Yang, L., Gao, B., Li, R., and  
1012 Xu, B.: Evaluating the “2+26” regional strategy for air quality improvement during two air pollution  
1013 alerts in Beijing: variations in PM<sub>2.5</sub> concentrations, source apportionment, and the relative contribution  
1014 of local emission and regional transport, *Atmos. Chem. Phys.*, 19, 6879-6891,  
1015 <https://doi.org/10.5194/acp-19-6879-2019>, 2019.

1016 Cheng, J., Su, J., Cui, T., Li, X., Dong, X., Sun, F., Yang, Y., Tong, D., Zheng, Y., Li, Y., Li, J., Zhang,  
1017 Q., and He, K.: Dominant role of emission reduction in PM<sub>2.5</sub> air quality improvement in Beijing during  
1018 2013-2017: a model-based decomposition analysis, *Atmos. Chem. Phys.*, 19, 6125-6146,  
1019 <https://doi.org/10.5194/acp-19-6125-2019>, 2019a.

1020 Cheng, N., Li, R., Xu, C., Chen, Z., Chen, D., Meng, F., Cheng, B., Ma, Z., Zhuang, Y., He, B., and Gao,  
1021 B.: Ground ozone variations at an urban and a rural station in Beijing from 2006 to 2017: Trend,

1022 meteorological influences and formation regimes, *J. Cleaner Prod.*, 235, 11-20,  
1023 <https://doi.org/10.1016/j.jclepro.2019.06.204>, 2019b.

1024 Dickerson, R. R., Kondragunta, S., Stenchikov, G., Civerolo, K. L., Doddridge, B. G., and Holben, B.  
1025 N.: The impact of aerosols on solar ultraviolet radiation and photochemical smog, *Science*, 278, 827-830,  
1026 <https://doi.org/10.1126/science.278.5339.827>, 1997.

1027 Ding, A., Huang, X., Nie, W., Chi, X., Xu, Z., Zheng, L., Xu, Z., Xie, Y., Qi, X., Shen, Y., Sun, P., Wang,  
1028 J., Wang, L., Sun, J., Yang, X.-q., Qin, W., Zhang, X., Cheng, W., Liu, W., Pan, L., and Fu, C.: Significant  
1029 reduction of PM<sub>2.5</sub> in eastern China due to regional-scale emission control: evidence from SORPES in  
1030 2011–2018, *Atmos. Chem. Phys.*, 19, 11791–11801, [https://doi.org/https://doi.org/10.5194/acp-19-](https://doi.org/https://doi.org/10.5194/acp-19-11791-2019)  
1031 [11791-2019](https://doi.org/https://doi.org/10.5194/acp-19-11791-2019), 2019.

1032 Frischer, T., Studnicka, M., Gartner, C., Tauber, E., Horak, F., Veiter, A., Spengler, J., Kuhr, J., and  
1033 Urbanek, R.: Lung function growth and ambient ozone - A three-year population study in school children,  
1034 *Am. J. Resp. Cirt. Care*, 160, 390-396, <https://doi.org/10.1164/ajrccm.160.2.9809075>, 1999.

1035 **Gregory, L.: Cimel Sunphotometer (CSPHOT) Handbook, Office of Scientific & Technical Information**  
1036 **Technical Reports, <https://doi.org/10.2172/1020262>, 2011.**

1037 Han, L., Xiang, X., Zhang, H., Cheng, S., Wang, H., Wei, W., Wang, H., and Lang, J.: Insights into  
1038 submicron particulate evolution, sources and influences on haze pollution in Beijing, China, *Atmos.*  
1039 *Environ.*, 201, 360-368, <https://doi.org/10.1016/j.atmosenv.2018.12.045>, 2019.

1040 Harris, E., Sinha, B., van Pinxteren, D., Tilgner, A., Fomba, K. W., Schneider, J., Roth, A., Gnauk, T.,  
1041 Fahlbusch, B., Mertes, S., Lee, T., Collett, J., Foley, S., Borrmann, S., Hoppe, P., and Herrmann, H.:  
1042 Enhanced Role of Transition Metal Ion Catalysis During In-Cloud Oxidation of SO<sub>2</sub>, *Science*, 340, 727-  
1043 730, <https://doi.org/10.1126/science.1230911>, 2013.

1044 Hassan, I. A., Basahi, J. M., Ismail, I. M., and Habeebullah, T. M.: Spatial Distribution and Temporal  
1045 Variation in Ambient Ozone and Its Associated NO<sub>x</sub> in the Atmosphere of Jeddah City, Saudi Arabia,  
1046 *Aerosol Air. Qual. Res*, 13, 1712-1722, <https://doi.org/10.4209/aaqr.2013.01.0007>, 2013.

1047 He, S., and Carmichael, G. R.: Sensitivity of photolysis rates and ozone production in the troposphere to  
1048 aerosol properties, *J. Geophys. Res.: Atmos.*, 104, 26307-26324, <https://doi.org/10.1029/1999jd900789>,  
1049 1999.

1050 Hennigan, C. J., Miracolo, M. A., Engelhart, G. J., May, A. A., Presto, A. A., Lee, T., Sullivan, A. P.,

1051 McMeeking, G. R., Coe, H., Wold, C. E., Hao, W. M., Gilman, J. B., Kuster, W. C., de Gouw, J., Schichtel,  
1052 B. A., Collett, J. L., Jr., Kreidenweis, S. M., and Robinson, A. L.: Chemical and physical transformations  
1053 of organic aerosol from the photo-oxidation of open biomass burning emissions in an environmental  
1054 chamber, *Atmos. Chem. Phys.*, 11, 7669-7686, <https://doi.org/10.5194/acp-11-7669-2011>, 2011.

1055 Huang, X., Liu, Z., Liu, J., Hu, B., Wen, T., Tang, G., Zhang, J., Wu, F., Ji, D., Wang, L., and Wang, Y.:  
1056 Chemical characterization and source identification of PM<sub>2.5</sub> at multiple sites in the Beijing-Tianjin-  
1057 Hebei region, China, *Atmos. Chem. Phys.*, 17, 12941-12962, <https://doi.org/10.5194/acp-17-12941-2017>,  
1058 2017.

1059 Khoder, M. I.: Atmospheric conversion of sulfur dioxide to particulate sulfate and nitrogen dioxide to  
1060 particulate nitrate and gaseous nitric acid in an urban area, *Chemosphere*, 49, 675-684,  
1061 [https://doi.org/10.1016/s0045-6535\(02\)00391-0](https://doi.org/10.1016/s0045-6535(02)00391-0), 2002.

1062 Kong, L., Du, C., Zhanzakova, A., Cheng, T., Yang, X., Wang, L., Fu, H., Chen, J., and Zhang, S.: Trends  
1063 in heterogeneous aqueous reaction in continuous haze episodes in suburban Shanghai: An in-depth case  
1064 study, *Sci. Total Environ.*, 634, 1192-1204, <https://doi.org/10.1016/j.scitotenv.2018.04.086>, 2018.

1065 Li, L., Chen, C. H., Huang, C., Huang, H. Y., Zhang, G. F., Wang, Y. J., Wang, H. L., Lou, S. R., Qiao,  
1066 L. P., Zhou, M., Chen, M. H., Chen, Y. R., Streets, D. G., Fu, J. S., and Jang, C. J.: Process analysis of  
1067 regional ozone formation over the Yangtze River Delta, China using the Community Multi-scale Air  
1068 Quality modeling system, *Atmos. Chem. Phys.*, 12, 10971-10987, [https://doi.org/10.5194/acp-12-10971-](https://doi.org/10.5194/acp-12-10971-2012)  
1069 2012, 2012.

1070 Li, W., Liu, X., Zhang, Y., Tan, Q., Feng, M., Song, M., Hui, L., Qu, Y., An, J., and Gao, H.: Insights into  
1071 the phenomenon of an explosive growth and sharp decline in haze: A case study in Beijing, *J. Environ.*  
1072 *Sci. (China)*, 84, 122-132, <https://doi.org/10.1016/j.jes.2019.04.015>, 2019.

1073 Liu, G., Xin, J., Wang, X., Si, R., Ma, Y., Wen, T., Zhao, L., Zhao, D., Wang, Y., and Gao, W.: Impact of  
1074 the coal banning zone on visibility in the Beijing-Tianjin-Hebei region, *Sci. Total Environ.*, 692, 402-  
1075 410, <https://doi.org/10.1016/j.scitotenv.2019.07.006>, 2019a.

1076 Liu, H., Wang, X. M., Pang, J. M., and He, K. B.: Feasibility and difficulties of China's new air quality  
1077 standard compliance: PRD case of PM<sub>2.5</sub> and ozone from 2010 to 2025, *Atmos. Chem. Phys.*, 13, 12013-  
1078 12027, <https://doi.org/10.5194/acp-13-12013-2013>, 2013a.

1079 Liu, Q., Liu, T., Chen, Y., Xu, J., Gao, W., Zhang, H., and Yao, Y.: Effects of aerosols on the surface

1080 ozone generation via a study of the interaction of ozone and its precursors during the summer in Shanghai,  
1081 China, *Sci. Total Environ.*, 675, 235-246, <https://doi.org/10.1016/j.scitotenv.2019.04.121>, 2019b.

1082 Liu, X. G., Li, J., Qu, Y., Han, T., Hou, L., Gu, J., Chen, C., Yang, Y., Liu, X., Yang, T., Zhang, Y., Tian,  
1083 H., and Hu, M.: Formation and evolution mechanism of regional haze: a case study in the megacity  
1084 Beijing, China, *Atmos. Chem. Phys.*, 13, 4501-4514, <https://doi.org/10.5194/acp-13-4501-2013>, 2013b.

1085 Liu, Z., Hu, B., Ji, D., Cheng, M., Gao, W., Shi, S., Xie, Y., Yang, S., Gao, M., Fu, H., Chen, J., and Wang,  
1086 Y.: Characteristics of fine particle explosive growth events in Beijing, China: Seasonal variation,  
1087 chemical evolution pattern and formation mechanism, *Sci. Total Environ.*, 687, 1073-1086,  
1088 <https://doi.org/10.1016/j.scitotenv.2019.06.068>, 2019c.

1089 Lu, X., Zhang, L., Chen, Y., Zhou, M., Zheng, B., Li, K., Liu, Y., Lin, J., Fu, T. M., and Zhang, Q.:  
1090 Exploring 2016–2017 surface ozone pollution over China: source contributions and meteorological  
1091 influences, *Atmos. Chem. Phys.*, 19, 8339-8361, <https://doi.org/10.5194/acp-19-8339-2019>, 2019.

1092 Luan, T., Guo, X., Guo, L., and Zhang, T.: Quantifying the relationship between PM<sub>2.5</sub> concentration,  
1093 visibility and planetary boundary layer height for long-lasting haze and fog-haze mixed events in Beijing,  
1094 *Atmos. Chem. Phys.*, 18, 203-225, <https://doi.org/10.5194/acp-18-203-2018>, 2018.

1095 Martin, R. V., Jacob, D. J., Yantosca, R. M., Chin, M., and Ginoux, P.: Global and regional decreases in  
1096 tropospheric oxidants from photochemical effects of aerosols, *J. Geophys. Res.: Atmos.*, 108,  
1097 <https://doi.org/10.1029/2002jd002622>, 2003.

1098 Ming, L., Jin, L., Li, J., Fu, P., Yang, W., Liu, D., Zhang, G., Wang, Z., and Li, X.: PM<sub>2.5</sub> in the Yangtze  
1099 River Delta, China: Chemical compositions, seasonal variations, and regional pollution events, *Environ.*  
1100 *Pollut.*, 223, 200-212, <https://doi.org/10.1016/j.envpol.2017.01.013>, 2017.

1101 Muenkel, C., Eresmaa, N., Rasanen, J., and Karppinen, A.: Retrieval of mixing height and dust  
1102 concentration with lidar ceilometer, *Bound-Lay. Meteorol.*, 124, 117-128,  
1103 <https://doi.org/10.1007/s10546-006-9103-3>, 2007.

1104 Ng, N. L., Herndon, S. C., Trimborn, A., Canagaratna, M. R., Croteau, P. L., Onasch, T. B., Sueper, D.,  
1105 Worsnop, D. R., Zhang, Q., Sun, Y. L., and Jayne, J. T.: An Aerosol Chemical Speciation Monitor (ACSM)  
1106 for Routine Monitoring of the Composition and Mass Concentrations of Ambient Aerosol, *Aerosol Sci.*  
1107 *Tech.*, 45, 780-794, <https://doi.org/10.1080/02786826.2011.560211>, 2011.

1108 Orrling, D., Fitzgerald, E., Ivanov, A., and Molina, M.: Enhanced sulfate formation on ozone-exposed

1109 soot, *J. Aerosol Sci.*, 42, 615-620, <https://doi.org/10.1016/j.jaerosci.2011.04.004>, 2011.

1110 Pathak, R. K., Wu, W. S., and Wang, T.: Summertime PM<sub>2.5</sub> ionic species in four major cities of China:  
1111 nitrate formation in an ammonia-deficient atmosphere, *Atmos. Chem. Phys.*, 9, 1711-1722,  
1112 <https://doi.org/10.5194/acp-9-1711-2009>, 2009.

1113 Pathak, R. K., Wang, T., and Wu, W. S.: Nighttime enhancement of PM<sub>2.5</sub> nitrate in ammonia-poor  
1114 atmospheric conditions in Beijing and Shanghai: Plausible contributions of heterogeneous hydrolysis of  
1115 N<sub>2</sub>O<sub>5</sub> and HNO<sub>3</sub> partitioning, *Atmos. Environ.*, 45, 1183-1191,  
1116 <https://doi.org/10.1016/j.atmosenv.2010.09.003>, 2011.

1117 Petzold, A., and Schonlinner, M.: Multi-angle absorption photometry - a new method for the  
1118 measurement of aerosol light absorption and atmospheric black carbon, *J. Aerosol Sci.*, 35, 421-441,  
1119 <https://doi.org/10.1016/j.jaerosci.2003.09.005>, 2004.

1120 Richards, L. W.: comments on the oxidation of NO<sub>2</sub> to nitrate- day and night, *Atmos. Environ.*, 17, 397-  
1121 402, [https://doi.org/10.1016/0004-6981\(83\)90057-4](https://doi.org/10.1016/0004-6981(83)90057-4), 1983.

1122 Russell, A. G., Cass, G. R., and Seinfeld, J. H.: On some aspects of nighttime atmospheric chemistry,  
1123 *Environ. Sci. Technol.*, 20, 1167-1172, <https://doi.org/10.1021/es00153a013>, 1986.

1124 Seinfeld, J. H.: Atmospheric chemistry and physics of air pollution, Wiley, new York,  
1125 <https://doi.org/10.1021/es00151a602>, 1986.

1126 Seinfeld, J. H., and Pandis, S. N.: Atmospheric chemistry and physics: from air pollution to climate  
1127 change, John Wiley & Sons, Inc, <https://doi.org/10.1080/00139157.1999.10544295>, 2006.

1128 Sharma, P., Kuniyal, J. C., Chand, K., Guleria, R. P., Dhyani, P. P., and Chauhan, C.: Surface ozone  
1129 concentration and its behaviour with aerosols in the northwestern Himalaya, India, *Atmos. Environ.*, 71,  
1130 44-53, <https://doi.org/10.1016/j.atmosenv.2012.12.042>, 2013.

1131 Shi, C., Wang, S., Liu, R., Zhou, R., Li, D., Wang, W., Li, Z., Cheng, T., and Zhou, B.: A study of aerosol  
1132 optical properties during ozone pollution episodes in 2013 over Shanghai, China, *Atmos. Res.*, 153, 235-  
1133 249, <https://doi.org/10.1016/j.atmosres.2014.09.002>, 2015.

1134 Sillman, S.: The relation between ozone, NO<sub>x</sub> and hydrocarbons in urban and polluted rural  
1135 environments, *Atmos. Environ.*, 33, 1821-1845, [https://doi.org/10.1016/s1352-2310\(98\)00345-8](https://doi.org/10.1016/s1352-2310(98)00345-8), 1999.

1136 Stull, R. B.: An Introduction to Boundary Layer Meteorology, [https://doi.org/10.1007/978-94-009-3027-](https://doi.org/10.1007/978-94-009-3027-8)  
1137 8 10, 1988.

1138 Stone, R. S., Anderson, G. P., Shettle, E. P., Andrews, E., Loukachine, K., Dutton, E. G., Schaaf, C., and  
1139 Roman, M. O., III: Radiative impact of boreal smoke in the Arctic: Observed and modeled, *J. Geophys.*  
1140 *Res.: Atmos.*, 113, <https://doi.org/10.1029/2007jd009657>, 2008.

1141 Su, F., Gao, Q., Zhang, Z., Ren, Z., and Yang, X.: Transport pathways of pollutants from outside in  
1142 atmosphere boundary layer, *Res. Environ. Sci.*, 17(1), 26-29,40, <https://doi.org/10.3321/j.issn:1001-6929.2004.01.005>, 2004.

1144 Sun, Y., Zhuang, G., Tang, A., Wang, Y., and An, Z.: Chemical characteristics of PM<sub>2.5</sub> and PM<sub>10</sub> in  
1145 haze-fog episodes in Beijing, *Environ. Sci. Technol.*, 40, 3148-3155, <https://doi.org/10.1021/es051533g>,  
1146 2006.

1147 Sun, Y., Wang, Z., Dong, H., Yang, T., Li, J., Pan, X., Chen, P., and Jayne, J. T.: Characterization of  
1148 summer organic and inorganic aerosols in Beijing, China with an Aerosol Chemical Speciation Monitor,  
1149 *Atmos. Environ.*, 51, 250-259, <https://doi.org/10.1016/j.atmosenv.2012.01.013>, 2012.

1150 Sun, Y. L., Wang, Z. F., Du, W., Zhang, Q., Wang, Q. Q., Fu, P. Q., Pan, X. L., Li, J., Jayne, J., and  
1151 Worsnop, D. R.: Long-term real-time measurements of aerosol particle composition in Beijing, China:  
1152 seasonal variations, meteorological effects, and source analysis, *Atmos. Chem. Phys.*, 15, 10149-10165,  
1153 <https://doi.org/10.5194/acp-15-10149-2015>, 2015.

1154 Tang, G., Zhang, J., Zhu, X., Song, T., Muenkel, C., Hu, B., Schaefer, K., Liu, Z., Zhang, J., Wang, L.,  
1155 Xin, J., Suppan, P., and Wang, Y.: Mixing layer height and its implications for air pollution over Beijing,  
1156 China, *Atmos. Chem. Phys.*, 16, 2459-2475, <https://doi.org/10.5194/acp-16-2459-2016>, 2016.

1157 Tie, X., Brasseur, G., Emmons, L., Horowitz, L., and Kinnison, D.: Effects of aerosols on tropospheric  
1158 oxidants: A global model study, *J. Geophys. Res.: Atmos.*, 106, 22931-22964,  
1159 <https://doi.org/10.1029/2001jd900206>, 2001.

1160 Tie, X. X., Madronich, S., Walters, S., Edwards, D. P., Ginoux, P., Mahowald, N., Zhang, R. Y., Lou, C.,  
1161 and Brasseur, G.: Assessment of the global impact of aerosols on tropospheric oxidants, *J. Geophys. Res.:*  
1162 *Atmos.*, 110, <https://doi.org/10.1029/2004jd005359>, 2005.

1163 Toh, Y. Y., Lim, S. F., and von Glasow, R.: The influence of meteorological factors and biomass burning  
1164 on surface ozone concentrations at Tanah Rata, Malaysia, *Atmos. Environ.*, 70, 435-446,  
1165 <https://doi.org/10.1016/j.atmosenv.2013.01.018>, 2013.

1166 Trainer, M., Parrish, D. D., Goldan, P. D., Roberts, J., and Fehsenfeld, F. C.: Review of observation-

1167 based analysis of the regional factors influencing ozone concentrations, *Atmos. Environ.*, 34, 2045-2061,  
1168 [https://doi.org/10.1016/s1352-2310\(99\)00459-8](https://doi.org/10.1016/s1352-2310(99)00459-8), 2000.

1169 Wang, D., Zhou, B., Fu, Q., Zhao, Q., Zhang, Q., Chen, J., Yang, X., Duan, Y., and Li, J.: Intense  
1170 secondary aerosol formation due to strong atmospheric photochemical reactions in summer: observations  
1171 at a rural site in eastern Yangtze River Delta of China, *Sci. Total Environ.*, 571, 1454-1466,  
1172 <https://doi.org/10.1016/j.scitotenv.2016.06.212>, 2016.

1173 Wang, H., Lu, K., Chen, X., Zhu, Q., Chen, Q., Guo, S., Jiang, M., Li, X., Shang, D., Tan, Z., Wu, Y.,  
1174 Wu, Z., Zou, Q., Zheng, Y., Zeng, L., Zhu, T., Hu, M., and Zhang, Y.: High N<sub>2</sub>O<sub>5</sub> Concentrations  
1175 Observed in Urban Beijing: Implications of a Large Nitrate Formation Pathway, *Environ. Sci. Tech. Lett.*,  
1176 4, 416-420, <https://doi.org/10.1021/acs.estlett.7b00341>, 2017a.

1177 Wang, L., Zhang, F., Pilot, E., Yu, J., Nie, C., Holdaway, J., Yang, L., Li, Y., Wang, W., Vardoulakis, S.,  
1178 and Krafft, T.: Taking Action on Air Pollution Control in the Beijing-Tianjin-Hebei (BTH) Region:  
1179 Progress, Challenges and Opportunities, *Int. J. Env. Res. Pub. He.*, 15,  
1180 <https://doi.org/10.3390/ijerph15020306>, 2018.

1181 Wang, L., Liu, J., Gao, Z., Li, Y., Huang, M., Fan, S., Zhang, X., Yang, Y., Miao, S., Zou, H., Sun, Y.,  
1182 Chen, Y., and Yang, T.: Vertical observations of the atmospheric boundary layer structure over Beijing  
1183 urban area during air pollution episodes, *Atmos. Chem. Phys.*, 19, 6949-6967,  
1184 <https://doi.org/10.5194/acp-19-6949-2019>, 2019a.

1185 Wang, T., Xue, L., Brimblecombe, P., Lam, Y. F., Li, L., and Zhang, L.: Ozone pollution in China: A  
1186 review of concentrations, meteorological influences, chemical precursors, and effects, *Sci. Total Environ.*,  
1187 575, 1582-1596, <https://doi.org/10.1016/j.scitotenv.2016.10.081>, 2017b.

1188 Wang, T., Xue, L. K., Brimblecombe, P., Lam, Y. F., Li, L., and Zhang, L.: Ozone pollution in China: A  
1189 review of concentrations, meteorological influences, chemical precursors, and effects, *Sci. Total Environ.*,  
1190 575, 1582-1596, <https://doi.org/10.1016/j.scitotenv.2016.10.081>, 2017c.

1191 Wang, W., Li, X., Shao, M., Hu, M., Zeng, L., Wu, Y., and Tan, T.: The impact of aerosols on photolysis  
1192 frequencies and ozone production in Beijing during the 4-year period 2012–2015, *Atmos. Chem. Phys.*,  
1193 19, 9413-9429, <https://doi.org/10.5194/acp-19-9413-2019>, 2019b.

1194 Wang, X., Zhang, Y., Chen, H., Yang, X., Chen, J., and Geng, F.: Particulate Nitrate Formation in a Highly  
1195 Polluted Urban Area: A Case Study by Single-Particle Mass Spectrometry in Shanghai, *Environ. Sci.*



1196 Technol., 43, 3061-3066, <https://doi.org/10.1021/es8020155>, 2009.

1197 Wang, X., Wang, W., Yang, L., Gao, X., Nie, W., Yu, Y., Xu, P., Zhou, Y., and Wang, Z.: The secondary  
1198 formation of inorganic aerosols in the droplet mode through heterogeneous aqueous reactions under haze  
1199 conditions, *Atmos. Environ.*, 63, 68-76, <https://doi.org/10.1016/j.atmosenv.2012.09.029>, 2012.

1200 Wang, Y., Zhuang, G., Zhang, X., Huang, K., Xua, C., Tang, A., Chen, J., and An, Z.: The ion chemistry,  
1201 seasonal cycle, and sources of PM<sub>2.5</sub> and TSP aerosol in Shanghai, *Atmos. Environ.*, 40, 2935-2952,  
1202 <https://doi.org/10.1016/j.atmosenv.2005.12.051>, 2006.

1203 Wang, Y., Zhang, Q. Q., He, K., Zhang, Q., and Chai, L.: Sulfate-nitrate-ammonium aerosols over China:  
1204 response to 2000-2015 emission changes of sulfur dioxide, nitrogen oxides, and ammonia, *Atmos. Chem.*  
1205 *Phys.*, 13, 2635-2652, <https://doi.org/10.5194/acp-13-2635-2013>, 2013.

1206 Wang, Z., Pan, X., Uno, I., Li, J., Wang, Z., Chen, X., Fu, P., Yang, T., Kobayashi, H., Shimizu, A.,  
1207 Sugimoto, N., and Yamamoto, S.: Significant impacts of heterogeneous reactions on the chemical  
1208 composition and mixing state of dust particles: A case study during dust events over northern China,  
1209 *Atmos. Environ.*, 159, 83-91, <https://doi.org/10.1016/j.atmosenv.2017.03.044>, 2017d.

1210 Wen, L., Xue, L. K., Wang, X. F., Xu, C. H., Chen, T. S., Yang, L. X., Wang, T., Zhang, Q. Z., and Wang,  
1211 W. X.: Summertime fine particulate nitrate pollution in the North China Plain: increasing trends,  
1212 formation mechanisms and implications for control policy, *Atmos. Chem. Phys.*, 18, 11261-11275,  
1213 <https://doi.org/10.5194/acp-18-11261-2018>, 2018.

1214 Wilcox, E. M., Thomas, R. M., Praveen, P. S., Pistone, K., Bender, F. A. M., and Ramanathan, V.: Black  
1215 carbon solar absorption suppresses turbulence in the atmospheric boundary layer, *Proc. Natl. Acad. Sci.*  
1216 *U. S. A.*, 113, 11794-11799, <https://doi.org/10.1073/pnas.1525746113>, 2016.

1217 Wilson Jr, Wm. E., Levy, Arthur., and Wimmer, D.B.: A study of sulfur dioxide in photochemical smog,  
1218 *J. Air Pollut. Control Assoc.*, 22(1), 27-32, <https://doi.org/10.1080/00022470.1972.10469605>, 1972.

1219 Yao, X. H., Chan, C. K., Fang, M., Cadle, S., Chan, T., Mulawa, P., He, K. B., and Ye, B. M.: The water-  
1220 soluble ionic composition of PM<sub>2.5</sub> in Shanghai and Beijing, China, *Atmos. Environ.*, 36, 4223-4234,  
1221 [https://doi.org/10.1016/s1352-2310\(02\)00342-4](https://doi.org/10.1016/s1352-2310(02)00342-4), 2002.

1222 Zeng, P., Lyu, X. P., Guo, H., Cheng, H. R., Jiang, F., Pan, W. Z., Wang, Z. W., Liang, S. W., and Hu, Y.  
1223 Q.: Causes of ozone pollution in summer in Wuhan, Central China, *Environ. Pollut.*, 241, 852-861,  
1224 <https://doi.org/10.1016/j.envpol.2018.05.042>, 2018.

1225 Zhao, D., Xin, J., Gong, C., Quan, J., Liu, G., Zhao, W., Wang, Y., Liu, Z., and Song, T.: The formation  
1226 mechanism of air pollution episodes in Beijing city: Insights into the measured feedback between aerosol  
1227 radiative forcing and the atmospheric boundary layer stability, *Sci. Total Environ.*, 692, 371-381,  
1228 <https://doi.org/10.1016/j.scitotenv.2019.07.255>, 2019.

1229 Zhong, J., Zhang, X., Wang, Y., Sun, J., Zhang, Y., Wang, J., Tan, K., Shen, X., Che, H., Zhang, L., Zhang,  
1230 Z., Qi, X., Zhao, H., Ren, S., and Li, Y.: Relative Contributions of Boundary-Layer Meteorological  
1231 Factors to the Explosive Growth of PM<sub>2.5</sub> during the Red-Alert Heavy Pollution Episodes in Beijing in  
1232 December 2016, *J. Meteorol. Res.*, 31, 809-819, <https://doi.org/10.1007/s13351-017-7088-0>, 2017.

1233 Zhong, J., Zhang, X., Dong, Y., Wang, Y., Liu, C., Wang, J., Zhang, Y., and Che, H.: Feedback effects of  
1234 boundary-layer meteorological factors on cumulative explosive growth of PM<sub>2.5</sub> during winter heavy  
1235 pollution episodes in Beijing from 2013 to 2016, *Atmos. Chem. Phys.*, 18, 247-258,  
1236 <https://doi.org/10.5194/acp-18-247-2018>, 2018.

1237 Zhong, J., Zhang, X., Wang Y., Wang J., Shen X., Zhang H., Wang T., Xie Z., Liu C., Zhang H., Zhao T.,  
1238 Sun J., Fan S., Gao Z., Li Y., and Wang L.: The two-way feedback mechanism between unfavorable  
1239 meteorological conditions and cumulative aerosol pollution in various haze regions of China, *Atmos.*  
1240 *Chem. Phys.*, 19, 3287–3306, <https://doi.org/10.5194/acp-19-3287-2019>, 2019.

1241 Zhu, X., Tang, G., Lv, F., Hu, B., Cheng, M., Muenkel, C., Schafer, K., Xin, J., An, X., Wang, G., Li, X.,  
1242 and Wang, Y.: The spatial representativeness of mixing layer height observations in the North China Plain,  
1243 *Atmos. Res.*, 209, 204-211, <https://doi.org/10.1016/j.atmosres.2018.03.019>, 2018.